

Contrastive Conditional Transport for Representation Learning

Huangjie Zheng^{*1} Xu Chen^{* 234} Jiangchao Yao⁴ Hongxia Yang⁴ Chunyuan Li⁵

Ya Zhang² Hao Zhang⁶ Ivor W. Tsang³ Jingren Zhou⁴ Mingyuan Zhou¹

¹The University of Texas at Austin ²Shanghai Jiao Tong University

³University of Technology Sydney ⁴Alibaba Group ⁵Microsoft Research ⁶Cornell University

Abstract

Contrastive learning (CL) has achieved remarkable success in learning data representations without label supervision. However, the conventional CL loss is sensitive to how many negative samples are included and how they are selected. This paper proposes contrastive conditional transport (CCT) that defines its CL loss over dependent sample-query pairs, which in practice is realized by drawing a random query, randomly selecting positive and negative samples, and contrastively reweighting these samples according to their distances to the query, exerting a greater force to both pull more distant positive samples towards the query and push closer negative samples away from the query. Theoretical analysis shows that this unique contrastive reweighting scheme helps in the representation space to both align the positive samples with the query and reduce the mutual information between the negative sample and query. Extensive large-scale experiments on standard vision tasks show that CCT not only consistently outperforms existing methods on benchmark datasets in contrastive representation learning, but also provides interpretable contrastive weights and latent representations. PyTorch code will be provided.

1 Introduction

The classical contrastive loss (Oord et al., 2018; Poole et al., 2018) has achieved remarkable success in representation learning, benefiting downstream tasks in a variety of areas (Misra & Maaten, 2020; He et al., 2020; Chen et al., 2020a; Fang & Xie, 2020; Giorgi et al., 2020). The intuition of the contrastive loss is that given a query, its positive sample needs to be close, while the negative samples need to be far away in the representation space, for which the unit hypersphere is the most common assumption (Wang et al., 2017; Davidson et al., 2018). This learning scheme encourages the encoder to learn representations that are invariant to unnecessary details, and uniformly distributed on the hypersphere to maximally preserve relevant information (Hjelm et al., 2018; Tian et al., 2019; Bachman et al., 2019; Wang & Isola, 2020).

A notable concern of the conventional contrastive loss is that the query’s positive and negative samples are often uniformly sampled and equally treated in the comparison, which results in an inefficient estimation and limits the performance of learned representations (Saunshi et al., 2019b; Chuang et al., 2020). As illustrated in Figure 1, given a query, the conventional CL methods usually randomly take one positive sample to form the positive pair and equally treat all the other negative pairs, regardless of how informative a sample is to the query. Thus, there is no guarantee for the uniformity of the representations of the samples on the hypersphere, to address which recent works propose to more carefully choose the samples to form the contrastive loss *e.g.*, strong augmentations or hard example synthesis (Chen et al., 2020a; Tian et al., 2019; Chuang et al., 2020; Kalantidis et al., 2020; Wu et al., 2021). Besides carefully selecting the samples, another way is to consider the importance of each sample according to how informative it is to the query. Below we propose a novel method to unite these two seemingly different ideas.

In this paper, we propose contrastive conditional transport (CCT) as a novel CL framework, which differs from previous ones in modeling the dependence of both the positive and negative samples on the query. CCT integrates CL into conditional transport (Zheng & Zhou, 2020), a framework that measures the difference between two implicit probability distributions given their empirical samples. It models the relation between the samples and query with a point-to-point transport cost function and two distinct conditional transport maps determining the probability of transporting a positive or negative sample given the query. Intuitively, as in Figure 1, if a selected positive sample is far from the query, it indicates the encoder does not sufficiently capture some information, and CCT will place more attention to transport this positive sample towards the query. Conversely, if a selected negative

^{*}Equal contribution

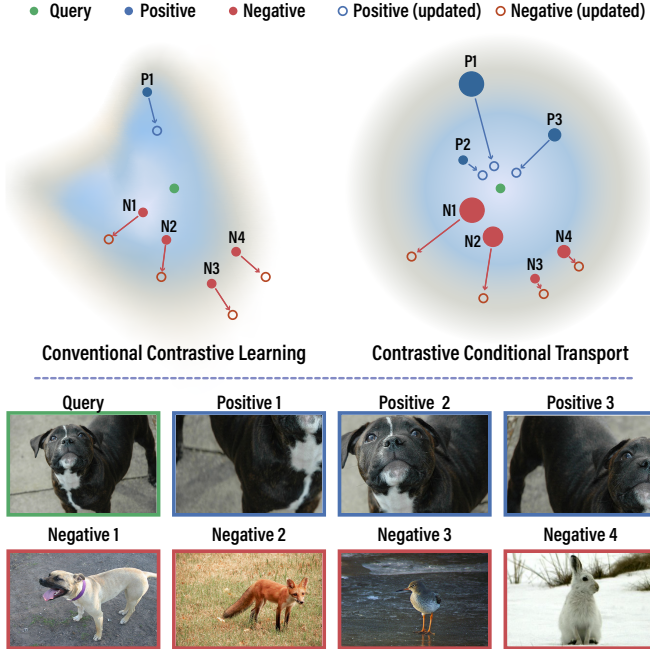


Figure 1: Comparison of conventional contrastive learning (CL) and the proposed contrastive conditional transport (CCT), illustrated in the latent space (*Top*) and data space (*Bottom*). For conventional CL, given a query, the model randomly takes one positive sample to form a positive pair and compares it against multiple negative pairs, with all samples equally treated. For CCT, using multiple positive and negative pairs, the weight of a sample (indicated by point scale) is contrastively computed to more strongly pull more distant positive samples towards the query and push closer negative samples away from the query, making the update adaptive to samples and encouraging uniformity.

sample is too close to the query, it indicates the encoder is challenging to distinguish them, and CCT will emphasize more on transporting this negative sample away from the query.

Drawing random samples dependent on the query under the conditional transport map, however, is often intractable. In practice, CCT is able to follow the convention to draw random positive samples that are conditionally independent of the query and independent negative samples, but distinct from conventional CL methods, these samples are contrastively reweighted according to their distances to the query and hence no longer treated equally.

Our main contributions include: 1) CCT formulates the importance of positive and negative samples with conditional transport maps, with the weight of a sample indicating how informative it is to the query. Compared to conventional CL methods, CCT can naturally take multiple positive samples at a time and contrastively weigh each positive and negative sample. 2) CCT defines the expected transport cost as its loss function and produces useful representations by minimizing the expected transport cost of positive samples while maximizing that of negative samples. In this view, the conventional CL methods could be considered as a special case of CCT where we have only one positive pair and uniform transport. 3) We provide both theoretical and empirical analysis to show that the unique reweighting scheme helps to align the positive samples with the query and reduce the mutual information between the negative samples and query. Our experiments show that CCT consistently outperforms conventional CL methods, achieving state-of-the-art results on standard vision tasks over various benchmark datasets.

2 Related Work

Unsupervised Representation Learning. Plenty of unsupervised representation learning (Bengio et al., 2013) methods have been developed to learn good data representations, *e.g.*, PCA (Tipping & Bishop, 1999), RBM (Hinton & Salakhutdinov, 2006), VAE (Kingma & Welling, 2014). Among them, CL (Oord et al., 2018) is investigated as a lower bound of mutual information in early stage (Gutmann & Hyvärinen, 2010; Hjelm et al., 2018). Recently, many studies reveal that the effectiveness of CL is not just attributed to the maximization of mutual information (Tschanne et al., 2019; Tian et al., 2020a), motivating various works to demystify the contrastive learning scheme.

Contrastive Representation Learning. In computer vision tasks, SimCLR (Chen et al., 2020a;b) studies extensive augmentations for positive and negative samples and intra-batch-based negative sampling. A memory bank that caches representations (Wu et al., 2018) and a momentum

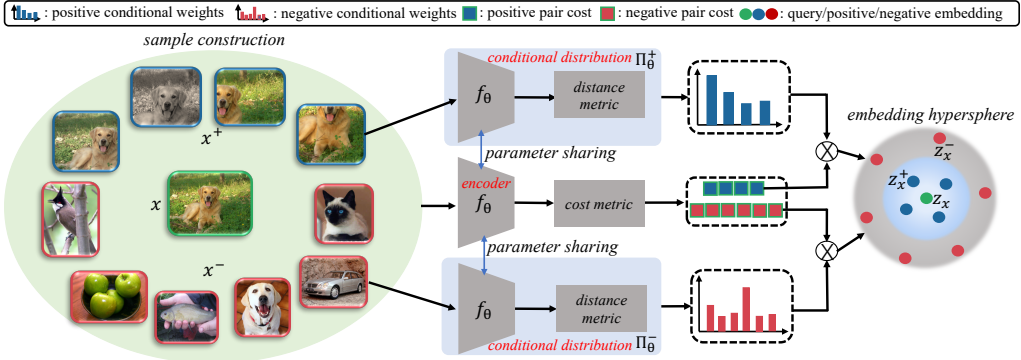


Figure 2: Illustration of CCT framework. The encoder extracts embeddings from samples and the conditional distributions indicate the transport maps for optimizing the transport cost in contrastive learning. The conditional weights are calculated according to the distance of a query \mathbf{x} and its contrastive samples $\mathbf{x}^+, \mathbf{x}^-$. \otimes means element-wise multiplication between costs and conditional weights.

update strategy are introduced to enable the usage of an enormous number of negative samples (He et al., 2020; Chen et al., 2020c). Apart from vision tasks, CL has been developed in learning representations for text (Logeswaran & Lee, 2018), sequential data (Oord et al., 2018; Hénaff et al., 2019), structural data like graphs (Sun et al., 2020; Li et al., 2019; Hassani & Khasahmadi, 2020; Velickovic et al., 2019), reinforcement learning (Srinivas et al., 2020), and few-shot scenarios (Khosla et al., 2020; Sylvain et al., 2020). Along with the success of these designs, works like Wang & Isola (2020) reveal the contrastive scheme is optimizing the alignment of positive samples and the uniformity of negative pairs in the limit of an infinite number of negative samples.

Sample Selection for CL. How to construct samples in CL has also been widely studied. For positive samples, Chen et al. (2020a;c) propose to apply perturbations in the images. Tian et al. (2019; 2020b) consider the image views in different modalities and minimize the irrelevant mutual information between them. Most of the works on negative selection observe the merits of using “hard” negative samples, motivating the introduction of additional techniques, such as Mixup and adversarial noise (Bose et al., 2018; Cherian & Aeron, 2020; Li et al., 2020). In a view that not all negative pairs are “true” negatives (Saunshi et al., 2019b), Chuang et al. (2020) propose a decomposition of the data distribution to approximate the true negative distribution. Wu et al. (2021) propose to use “neither too hard nor too easy” negative samples, and Robinson et al. (2021) apply Monte-Carlo sampling for selecting hard negative samples under the user’s control. As the transport map in CCT can be regarded as defining the sampling weights, our work is related to these works. An advantage is that the transport map of CCT is flexible and learnable, but not heuristically defined based on human prior knowledge.

3 Contrastive Conditional Transport

In CL, for observations $\mathbf{x}_{0:M} \sim p_{\text{data}}(\mathbf{x})$, we commonly assume that each \mathbf{x}_i can be transformed in certain ways, with the samples transformed from the same and different data regarded as positive and negative pairs, respectively. Specifically, denote $\mathcal{T}(\mathbf{x}_i, \epsilon_i)$ as a random transformation of \mathbf{x}_i , where $\epsilon_i \sim p(\epsilon)$ represents the randomness injected into the transformation. For example, in computer vision, ϵ_i usually represents a composition of random cropping, color jitter, Gaussian blurring, etc. For each \mathbf{x}_0 , with $\mathbf{x} = \mathcal{T}(\mathbf{x}_0, \epsilon_0)$ defined as the query, we sample a positive pair $(\mathbf{x}, \mathbf{x}^+)$, where $\mathbf{x}^+ = \mathcal{T}(\mathbf{x}_0, \epsilon^+)$, and M negative pairs $\{(\mathbf{x}, \mathbf{x}_i^-)\}_{1:M}$, where $\mathbf{x}_i^- = \mathcal{T}(\mathbf{x}_i, \epsilon_i^-)$. With an encoder $f_\theta : \mathbb{R}^n \rightarrow \mathcal{S}^{d-1}$, where we follow the convention to restrict the learned d -dimensional features with a unit norm, we desire to have similar and distinct representations for positive and negative pairs, respectively, via the contrastive loss as

$$\mathbb{E}_{(\mathbf{x}, \mathbf{x}^+, \mathbf{x}_i^-)} \left[-\ln \frac{e^{f_\theta(\mathbf{x})^\top f_\theta(\mathbf{x}^+)/\tau}}{e^{f_\theta(\mathbf{x})^\top f_\theta(\mathbf{x}^+)/\tau} + \sum_i e^{f_\theta(\mathbf{x}_i^-)^\top f_\theta(\mathbf{x})/\tau}} \right], \quad (1)$$

where $\tau \in \mathbb{R}^+$ denotes the temperature and $\mathbb{R}^+ := \{x : x > 0\}$. Note by construction, the positive sample \mathbf{x}^+ is independent of \mathbf{x} given \mathbf{x}_0 and the negative samples \mathbf{x}_i^- are independent of \mathbf{x} . Intuitively, this loss function encourages the encoder to not only pull the representation of a randomly selected positive sample closer to that of the query, but also push the representations of randomly selected negative samples away from that of the query.

3.1 Contrastive Uniform Transport

In the same spirit of (1), denoting $c(\mathbf{z}_1, \mathbf{z}_2)$ as the point-to-point cost of transporting between two vectors \mathbf{z}_1 and \mathbf{z}_2 , *e.g.*, the Euclidean distance $\|\mathbf{z}_1 - \mathbf{z}_2\|^2$ or the negative inner product $-\mathbf{z}_1^T \mathbf{z}_2$, we have considered contrastive uniform transport (CUT), whose objective is

$$\begin{aligned} \min_{\boldsymbol{\theta}} \{ & \mathbb{E}_{\mathbf{x}_0 \sim p_{data}(\mathbf{x})} \mathbb{E}_{\epsilon_0, \epsilon^+ \sim p(\epsilon)} [c(f_{\boldsymbol{\theta}}(\mathbf{x}), f_{\boldsymbol{\theta}}(\mathbf{x}^+))] \\ & - \mathbb{E}_{\mathbf{x}, \mathbf{x}^- \sim p(\mathbf{x})} [c(f_{\boldsymbol{\theta}}(\mathbf{x}), f_{\boldsymbol{\theta}}(\mathbf{x}^-))] \}. \end{aligned} \quad (2)$$

The intuition of CUT is to minimize/maximize the expected cost of moving between the representations of positive/negative samples, with the costs of all sample pairs being uniformly weighted. While (1) has been proven to be effective for representation learning, our experimental results do not find (2) to perform well, suggesting that the success of representation learning is not guaranteed by uniformly pulling positive samples closer and pushing negative samples away. However, there is clear room to improve CUT by either drawing correlated rather than independent sample pairs, or making independent samples be weighted differently.

3.2 CCT with Contrastive Reweighting

In what follows, leveraging the conditional transport (CT) framework of [Zheng & Zhou \(2020\)](#) that is used to measure the difference between two implicit probability distributions given their empirical samples, we generalize CUT to contrastive conditional transport (CCT). The proposed CCT also defines the expected transport cost as its loss function, but introduces a contrastive reweighting mechanism to put more emphasis on less similar positive pairs and more similar negative pairs. Specifically, viewing $\mathbf{x} = \mathcal{T}(\mathbf{x}_0, \epsilon_0)$ as the query, we define the conditional probability for transporting it to positive sample $\mathbf{x}^+ = \mathcal{T}(\mathbf{x}_0, \epsilon^+)$ as

$$\pi_{\boldsymbol{\theta}}^+(\mathbf{x}^+ | \mathbf{x}, \mathbf{x}_0) := \frac{e^{d_{t^+}(f_{\boldsymbol{\theta}}(\mathbf{x}), f_{\boldsymbol{\theta}}(\mathbf{x}^+))} p(\mathbf{x}^+ | \mathbf{x}_0)}{\int e^{d_{t^+}(f_{\boldsymbol{\theta}}(\mathbf{x}), f_{\boldsymbol{\theta}}(\mathbf{x}^+))} p(\mathbf{x}^+ | \mathbf{x}_0) d\mathbf{x}^+}, \quad (3)$$

where $f_{\boldsymbol{\theta}}(\cdot)$ is an encoder parameterized by $\boldsymbol{\theta}$ and $d_{t^+}(\cdot, \cdot)$ is a distance metric with temperature $t^+ \in \mathbb{R}^+$, *e.g.*, $d_{t^+}(\mathbf{z}_1, \mathbf{z}_2) = t^+ \|\mathbf{z}_1 - \mathbf{z}_2\|^2$. This construction makes it easier to transport \mathbf{x} to a positive sample that is more distant from it in their latent representation space. With (3), we can define the expected cost of transporting from a query to a positive sample as

$$\mathcal{C}^+ := \mathbb{E}_{\mathbf{x} \sim p(\mathbf{x})} \mathbb{E}_{\mathbf{x}^+ \sim \pi_{\boldsymbol{\theta}}^+(\cdot | \mathbf{x}, \mathbf{x}_0)} [c(f_{\boldsymbol{\theta}}(\mathbf{x}), f_{\boldsymbol{\theta}}(\mathbf{x}^+))], \quad (4)$$

which would more heavily weigh $c(f_{\boldsymbol{\theta}}(\mathbf{x}), f_{\boldsymbol{\theta}}(\mathbf{x}^+))$ if $f_{\boldsymbol{\theta}}(\mathbf{x})$ and $f_{\boldsymbol{\theta}}(\mathbf{x}^+)$ are further away from each other.

In contrast to (3), we define the conditional transport probability from query \mathbf{x} to a negative sample with

$$\pi_{\boldsymbol{\theta}}^-(\mathbf{x}^- | \mathbf{x}) := \frac{e^{-d_{t^-}(f_{\boldsymbol{\theta}}(\mathbf{x}), f_{\boldsymbol{\theta}}(\mathbf{x}^-))} p(\mathbf{x}^-)}{\int e^{-d_{t^-}(f_{\boldsymbol{\theta}}(\mathbf{x}), f_{\boldsymbol{\theta}}(\mathbf{x}^-))} p(\mathbf{x}^-) d\mathbf{x}^-}, \quad (5)$$

where $t^- \in \mathbb{R}^+$ controls the temperature. This construction makes it easier to transport query \mathbf{x} to a negative sample that is more closer from it in their latent representation space. With (5), we can define the expected cost of transporting from a query to a negative sample as

$$\mathcal{C}^- := \mathbb{E}_{\mathbf{x} \sim p(\mathbf{x})} \mathbb{E}_{\mathbf{x}^- \sim \pi_{\boldsymbol{\theta}}^-(\cdot | \mathbf{x})} [c(f_{\boldsymbol{\theta}}(\mathbf{x}), f_{\boldsymbol{\theta}}(\mathbf{x}^-))], \quad (6)$$

which would more heavily weigh $c(f_{\boldsymbol{\theta}}(\mathbf{x}), f_{\boldsymbol{\theta}}(\mathbf{x}^-))$ if $f_{\boldsymbol{\theta}}(\mathbf{x})$ and $f_{\boldsymbol{\theta}}(\mathbf{x}^-)$ are closer to each other.

Combining two different costs, we define the CCT loss as

$$\mathcal{L}_{\text{CCT}} = \mathcal{C}^+ - \mathcal{C}^-, \quad (7)$$

which shares the same intuition of conventional CL in pulling positive samples closer and pushing negative samples away in their representation space. However, CCT realizes this intuition by introducing the contrastive reweighting scheme on the point-to-point transport cost, with the scheme for positive samples contradicting to that for negative ones. The use of correlated sample pairs and two contradicting contrastive reweighting schemes clearly differs the CCT loss in (7) from the conventional CL loss in (1), which is typically formed with a single positive sample and multiple equally-weighted independent negative samples.

Distinction from CUT: Compared to CUT in (2) that uniformly weighs different pairs, CCT is distinct in considering the dependency between samples: as the latent-space distance between the query and its positive sample becomes larger, the conditional transport probability becomes higher, encouraging the encoder to focus more on the alignment of this pair. In the opposite, as the distance between the query and its negative sample becomes smaller, the conditional transport probability becomes higher, encouraging the encoder to push them away from each other.

Relationship with CT: The CT framework of [Zheng & Zhou \(2020\)](#) is primarily focused on measuring the divergence between two different distributions, which are referred to as the source and target distributions, respectively. It defines the expected CT cost from the source to target distributions as the forward CT, and that from the target to source as the backward CT. Minimizing the combined backward and forward CT cost, the primary goal is to optimize the target distribution to approximate the source distribution. By contrast, in CCT, since the marginal distributions of \mathbf{x} and \mathbf{x}^+ are the same and these of \mathbf{x} and \mathbf{x}^- are also the same, there is no need to differentiate the transport directions. In addition, the primary goal of CCT is not to regenerate the data but to learn $f_{\theta}(\cdot)$ that can provide good latent representations for downstream tasks.

3.3 Mini-batch based Stochastic Optimization

Under the CCT loss shown in (7), to make the learning of $f_{\theta}(\cdot)$ amenable to mini-batch SGD based optimization, we draw $(\mathbf{x}_i^{\text{data}}, \epsilon_i) \sim p_{\text{data}}(\mathbf{x})p(\epsilon)$ for $i = 1, \dots, M$ and then approximate the distribution of the query using an empirical distribution of M samples as

$$\hat{p}(\mathbf{x}) = \frac{1}{M} \sum_{i=1}^M \delta_{\mathbf{x}_i}, \quad \mathbf{x}_i = \mathcal{T}(\mathbf{x}_i^{\text{data}}, \epsilon_i).$$

Given query \mathbf{x}_i and with $\epsilon_{1:K} \stackrel{iid}{\sim} p(\epsilon)$, we approximate $p(\mathbf{x}_i^+ | \mathbf{x}_i^{\text{data}})$ for (3) with

$$\hat{p}(\mathbf{x}_i^+ | \mathbf{x}_i^{\text{data}}) = \frac{1}{K} \sum_{k=1}^K \delta_{\mathbf{x}_{ik}^+}, \quad \mathbf{x}_{ik}^+ = \mathcal{T}(\mathbf{x}_i^{\text{data}}, \epsilon_k). \quad (8)$$

We further approximate $p(\mathbf{x}_i^-)$ for (5) with

$$\hat{p}(\mathbf{x}_i^-) = \frac{1}{M-1} \sum_{j \neq i} \delta_{\mathbf{x}_j}. \quad (9)$$

Note we may improve the accuracy of $\hat{p}(\mathbf{x}_i^-)$ in (9) by adding previous queries into the support of this empirical distribution. Other more sophisticated ways to construct negative samples ([Ord et al., 2018; He et al., 2020; Khosla et al., 2020](#)) could also be adopted to define $\hat{p}(\mathbf{x}_i^-)$. We will elaborate these points when describing experiments.

Plugging (8) and (9) into (3) and (5), respectively, we can approximate the CT distributions as

$$\begin{aligned} \hat{\pi}_{\theta}^+(\mathbf{x}_i^+ | \mathbf{x}_i, \mathbf{x}_i^{\text{data}}) &:= \sum_{k=1}^K \frac{e^{d_{t+}(f_{\theta}(\mathbf{x}_i), f_{\theta}(\mathbf{x}_{ik}^+))}}{\sum_{k'=1}^K e^{d_{t+}(f_{\theta}(\mathbf{x}_i), f_{\theta}(\mathbf{x}_{ik'}^+))}} \delta_{\mathbf{x}_{ik}^+}; \\ \hat{\pi}_{\theta}^-(\mathbf{x}_i^- | \mathbf{x}_i) &:= \sum_{j \neq i} \frac{e^{-d_{t-}(f_{\theta}(\mathbf{x}_i), f_{\theta}(\mathbf{x}_j))}}{\sum_{j' \neq i} e^{-d_{t-}(f_{\theta}(\mathbf{x}_i), f_{\theta}(\mathbf{x}_{j'}^-))}} \delta_{\mathbf{x}_j}, \end{aligned}$$

which leads to the CCT loss as $\hat{\mathcal{L}}_{\text{CCT}} = \hat{\mathcal{C}}^+ - \hat{\mathcal{C}}^-$, where

$$\begin{aligned} \hat{\mathcal{C}}^+ &:= \frac{1}{M} \sum_{i=1}^M \sum_{k=1}^K \frac{e^{d_{t+}(f_{\theta}(\mathbf{x}_i), f_{\theta}(\mathbf{x}_{ik}^+))}}{\sum_{k'=1}^K e^{d_{t+}(f_{\theta}(\mathbf{x}_i), f_{\theta}(\mathbf{x}_{ik'}^+))}} \times c(f_{\theta}(\mathbf{x}_i), f_{\theta}(\mathbf{x}_{ik}^+)), \\ \hat{\mathcal{C}}^- &:= \frac{1}{M} \sum_{i=1}^M \sum_{j \neq i} \frac{e^{-d_{t-}(f_{\theta}(\mathbf{x}_i), f_{\theta}(\mathbf{x}_j))}}{\sum_{j' \neq i} e^{-d_{t-}(f_{\theta}(\mathbf{x}_i), f_{\theta}(\mathbf{x}_{j'}^-))}} \times c(f_{\theta}(\mathbf{x}_i), f_{\theta}(\mathbf{x}_j)). \end{aligned}$$

With this mini-batch based loss function, we can optimize θ via SGD using $\nabla_{\theta} \hat{\mathcal{L}}_{\text{CCT}}$.

Choice of $c(\cdot, \cdot)$, $d_{t+}(\cdot, \cdot)$ and $d_{t-}(\cdot, \cdot)$ There could be various choices for the point-to-point cost function $c(\cdot, \cdot)$, the distance metric $d_{t+}(\cdot, \cdot)$ in (4), and $d_{t-}(\cdot, \cdot)$ in (6). Considering the output of encoder f_{θ} are normalized vectors on the surface of a hypersphere, maximizing the inner product is equivalent to minimizing squared Euclidean distance. Without loss of generality, in our paper, we define them as

$$\begin{aligned} c(\mathbf{z}_1, \mathbf{z}_2) &= \|\mathbf{z}_1 - \mathbf{z}_2\|_2^2, \quad d_{t+}(\mathbf{z}_1, \mathbf{z}_2) = t^+ \|\mathbf{z}_1 - \mathbf{z}_2\|_2^2, \\ d_{t-}(\mathbf{z}_1, \mathbf{z}_2) &= t^- \|\mathbf{z}_1 - \mathbf{z}_2\|_2^2, \quad t^+, t^- \in \mathbb{R}^+. \end{aligned}$$

There are other choices for these two metrics and present interesting properties in CL. Below we show how these metrics vary and are related to some existing studies.

4 Property Analysis of CCT

In this section, we analyze the properties of CCT to reveal its effectiveness in representation learning.

Property 1. *The positive transport is optimized if and only if all positive samples of a query share the same representation as that query. More specifically, for query \mathbf{x} that is transformed from $\mathbf{x}_0 \sim p_{\text{data}}(\mathbf{x})$, its positive samples share the same representation with it, which means*

$$f_{\boldsymbol{\theta}}(\mathbf{x}^+) = f_{\boldsymbol{\theta}}(\mathbf{x}) \text{ for any } \mathbf{x}^+ \sim p(\mathbf{x}^+ | \mathbf{x}_0). \quad (10)$$

Lemma 1. *Without loss of generality, we define the cost function and metric in the conditional transport map as $c(\mathbf{z}_1, \mathbf{z}_2) = d(\mathbf{z}_1, \mathbf{z}_2) = \|\mathbf{z}_1 - \mathbf{z}_2\|_2^2$. Suppose all samples are equally likely in the prior, which means $p(\mathbf{x}) = p(\mathbf{x}^-)$ for any $\mathbf{x}, \mathbf{x}^- \stackrel{iid}{\sim} p(\mathbf{x})$, and their latent representations $\mathbf{z} = f_{\boldsymbol{\theta}}(\mathbf{x})$ and $\mathbf{z}^- = f_{\boldsymbol{\theta}}(\mathbf{x}^-)$ are also equally likely in the encoder space, which means $p(\mathbf{z}) = p(\mathbf{z}^-)$, then optimizing $\boldsymbol{\theta}$ to maximize the negative transport cost \mathcal{C}^- in (6) is the same as optimizing $\boldsymbol{\theta}$ to maximize the conditional differential entropy of \mathbf{x}^- given \mathbf{x} under the joint distribution $p(\mathbf{x})\pi_{\boldsymbol{\theta}}^-(\mathbf{x}^- | \mathbf{x})$, which can be expressed as*

$$\mathcal{H}(X^- | X) = \mathbb{E}_{\mathbf{x} \sim p(\mathbf{x})} \mathbb{E}_{\mathbf{x}^- \sim \pi_{\boldsymbol{\theta}}^-(\cdot | \mathbf{x})} [-\ln \pi_{\boldsymbol{\theta}}^-(\mathbf{x}^- | \mathbf{x})], \quad (11)$$

which is also the same as optimizing $\boldsymbol{\theta}$ to minimize the mutual information between \mathbf{x} and \mathbf{x}^- , expressed as

$$I(X; X^-) = \mathbb{E}_{\mathbf{x} \sim p(\mathbf{x})} \mathbb{E}_{\mathbf{x}^- \sim \pi_{\boldsymbol{\theta}}(\mathbf{x}^- | \mathbf{x})} \left[\ln \frac{\pi_{\boldsymbol{\theta}}(\mathbf{x}^- | \mathbf{x})}{p(\mathbf{x}^-)} \right]. \quad (12)$$

The above theorem suggests that to maximize \mathcal{C}^- , we can try to optimze $\boldsymbol{\theta}$ to minimize the mutual information of \mathbf{x} and \mathbf{x}^- drawn from $p(\mathbf{x})\pi_{\boldsymbol{\theta}}^-(\mathbf{x}^- | \mathbf{x})$, which is achieved when \mathbf{x} and \mathbf{x}^- become independent. We notice that one way to make this happen is to optimize $\boldsymbol{\theta}$ such that given $\mathbf{x} \sim p(\mathbf{x})$, $d(f_{\boldsymbol{\theta}}(\mathbf{x}), f_{\boldsymbol{\theta}}(\mathbf{x}^-))$ is equal to a constant for all $\mathbf{x}^- \sim p(\mathbf{x})$, which will make $\pi_{\boldsymbol{\theta}}^-(\mathbf{x}^- | \mathbf{x})$ defined in (5) be equal to $p(\mathbf{x}^-)$ for any \mathbf{x} . While in practice there may not exist an encoder to ensure both the uniform prior assumption on $p(\mathbf{z})$ and the assumption that $d(f_{\boldsymbol{\theta}}(\mathbf{x}), f_{\boldsymbol{\theta}}(\mathbf{x}^-))$ is a constant for different \mathbf{x}^- , the above analysis suggests that optimizing $\boldsymbol{\theta}$ to maximize \mathcal{C}^- will encourage some type of uniformity on the latent representations of independent samples.

Property 1 suggests that the optimal encoder produces representations invariant to the noisy details. From Lemma 1, the negative conditional transport map characterizes the solution, where an optimal encoder distributes samples with an equal distance to the query. Note that this optimum coincides with the conclusion of Wang & Isola (2020) that a perfect encoder will uniformly distribute samples on a hypersphere. Nonetheless, a distinction is that the optimum in CCT guarantees the distance is uniform with respect to (w.r.t.) the given query, on which a uniform prior is assumed. In a case where the query distribution is skewed, e.g., the number of samples in each class is imbalanced, uniformly distributing samples on a hypersphere may not be a good solution. We illustrate this with empirical experiments.

Relation to Classical Contrastive Scheme: Another natural question is how do the desired representations of CCT differ from those learned with classical CL. To analyze this, we formalize the relation between the conventional CL loss and proposed CCT loss.

Lemma 2. *As the number of negative samples M goes to infinity, the contribution of the negative samples to the CL loss shown in (1) can be expressed as*

$$\mathbb{E}_{\mathbf{x} \sim p(\mathbf{x})} \left[\ln \mathbb{E}_{\mathbf{x}^- \sim p(\mathbf{x}^-)} e^{f_{\boldsymbol{\theta}}(\mathbf{x}^-)^\top f_{\boldsymbol{\theta}}(\mathbf{x}) / \tau} \right],$$

adding which to the mutual information $I(X; X^-)$ in (12) becomes an upper bound of $-\mathcal{C}^-$ defined as in (6), which is the contribution of the negative samples to the CCT loss.

Note that the mutual information $I(X; X^-)$ appears in both Lemma 1 and 2. The interpretation is that as CCT optimize $\boldsymbol{\theta}$ to minimize $-\mathcal{C}^-$, it reduces the mutual information between a negative sample and the query, which consequently diminishes the difference between drawing \mathbf{x}^- that is dependent on \mathbf{x} , as done in CCT according to the conditional transport map $\pi_{\boldsymbol{\theta}}(\mathbf{x}^- | \mathbf{x})$, and drawing \mathbf{x}^- that is independent of \mathbf{x} , as done in conventional CL methods. When $\boldsymbol{\theta}$ has not been well optimized, the mutual information could be large, leading to a clear difference between the CCT loss, which considers the dependence of the negative sample on the query, and CL loss, which draws its negative samples independently of the query. Assuming the bound in Theorem 3 is tight, then minimizing the

$-\mathcal{C}^-$ component of the CCT loss is the same as minimizing the sum of the negative-sample related component of the CL loss and $I(X; X^-)$, which could enhance the robustness if the uniform prior assumption on \mathbf{x} is clearly violated.

Limitations of Uniform Sampling: The bias of uniform sampling has been recently discussed and the selection of negative samples plays an important role in addressing this issue in CL (Saunshi et al., 2019a; Chuang et al., 2020; Robinson et al., 2021; Wu et al., 2021). Our Lemma 1 and 2 also show the importance of modeling the dependence between the negative samples and query. The same spirit can be generalized to the selection of positive sample, which is equally important but less discussed in previous works. Note we can rewrite the positive transport cost \mathcal{C}^+ in (4) as

$$\mathbb{E}_{\mathbf{x}_0} \mathbb{E}_{\mathbf{x}, \mathbf{x}^+ \sim p(\cdot | \mathbf{x}_0)} \left[c(f_{\theta}(\mathbf{x}), f_{\theta}(\mathbf{x}^+)) \frac{\pi_{\theta}^+(\mathbf{x}^+ | \mathbf{x}, \mathbf{x}_0)}{p(\mathbf{x}^+ | \mathbf{x}_0)} \right],$$

which, if ignoring the dependence of \mathbf{x}^+ on \mathbf{x} and letting $c(f_{\theta}(\mathbf{x}), f_{\theta}(\mathbf{x}^+)) = -f_{\theta}(\mathbf{x})^\top f_{\theta}(\mathbf{x}^+)$, reduces to the numerator of the CL loss that is also known as the align loss (Wang & Isola, 2020), expressed as

$$\mathbb{E}_{\mathbf{x}_0 \sim p_{data}(\mathbf{x})} \mathbb{E}_{\mathbf{x}, \mathbf{x}^+ \sim p(\cdot | \mathbf{x}_0)} [-f_{\theta}(\mathbf{x})^\top f_{\theta}(\mathbf{x}^+)].$$

However, the positive pairs could have large difference in their distributions. For instance, given an image of a cat as the query, its positive sample could be either an image with different color style, or an image showing a body part after the crop. Constructing the dependence for positive pairs $\pi_{\theta}(\mathbf{x}^+ | \mathbf{x})$ is helpful, and using more positive pairs could make the estimation of dissimilarity more accurate. In the conventional CL loss, using multi-positive samples is feasible, but still requires to compare each of K positive pairs versus M negative pairs, e.g., CMC (Tian et al., 2019), which increases the complexity to $\mathcal{O}(K \times M)$ per query and ignores the dependence between positive samples. As for CCT, the computation complexity of positive and negative transport is $\mathcal{O}(K)$ and $\mathcal{O}(M)$, respectively. Moreover, CCT takes advantage of the transport maps to build the dependence between samples, which enhances the robustness when the data patterns are not uniformly distributed. We will illustrate this with empirical results.

5 Experiments and Analysis

We compare CCT’s performance with methods in two categories, according to their positive sampling size: $K = 1$ and $K = 4$. For methods with a single positive sample ($K = 1$), the baseline methods include the conventional CL loss (Oord et al., 2018; Logeswaran & Lee, 2018; Chen et al., 2020d; He et al., 2020), AlignUniform CL loss (AU-CL) (Wang & Isola, 2020), and the non-debiased version of the CL loss with hard negative sampling (HN-CL) (Robinson et al., 2021). In the case of $K = 4$, we take contrastive multi-view coding (CMC) loss (Tian et al., 2019) (align with our augmentation settings and use augmentation views instead of channels) as the comparison baseline. For a fair comparison, on each dataset, we keep for all methods the same experiment setting, e.g., learning-rate, mini-batch size, and training epochs. Please refer to Appendix B for other detailed experiment setups.

To evaluate the learned representations, following the widely used linear classification protocol, the pre-trained encoder is fixed as a proxy and a linear classifier is added on the top of the base feature encoder for classification. Following Wang & Isola (2020) and He et al. (2020), we conduct experiments on five image datasets of varying sizes, including CIFAR-10, CIFAR-100 (Hinton, 2007), and STL-10 (Coates et al., 2011) that are small-scale ones and ImageNet-100 and ImageNet-1K (Deng et al., 2009) that are large-scale ones. Note that ImageNet-100 has been recently used in CL works (Tian et al., 2019; Wang & Isola, 2020), where 100 classes are randomly selected from the standard ImageNet-1K dataset. For small-scale datasets, we follow SimCLR to construct negative samples as the views augmented from different images within a batch. Moreover, we create two class-imbalanced CIFAR datasets as empirical verification of our theoretical analysis. For large-scale datasets, we follow MoCo-v2 (Chen et al., 2020c) to maintain a queue of negative samples, updated with the momentum-based mechanism. Here we report the Top-1 validation accuracy on these datasets. The reported numbers for baselines are from their corresponding papers, or the best ones fine-tuned with the settings according to their corresponding papers.

5.1 Linear Classification on Small-scale Datasets

Classification accuracy: For small-scale datasets, following the setting in Wang & Isola (2020), all the methods are trained with an AlexNet-based encoder in 200 epochs. The results are summarized in Table 1. We can observe that in the case of $K = 1$, where the positive transport map of CCT degenerates, the performance of CCT is comparable and is slightly better than the baseline methods.

Table 1: The top-1 classification accuracy (%) of different contrastive objectives with SimCLR framework on small-scale datasets. All methods follow SimCLR setting and apply an AlexNet-based encoder. The results of CL and AU-CL on STL-10 are quoted from [Wang & Isola \(2020\)](#).

Methods	CIFAR-10	CIFAR-100	STL-10
CL	83.47	55.41	83.89
AU-CL	83.39	55.31	84.43
HN-CL	83.67	55.87	83.27
CCT ($K = 1$)	83.73	56.52	83.90
CMC ($K = 4$)	85.54	58.64	84.50
CCT ($K = 4$)	86.54	59.41	85.59

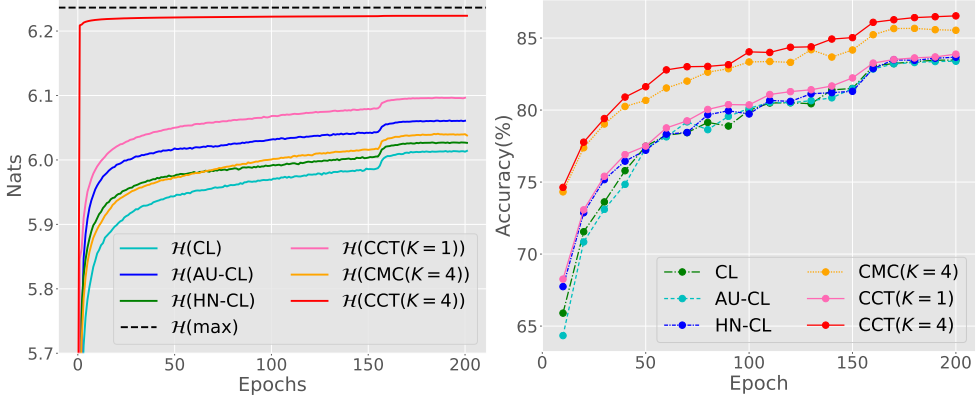


Figure 3: CIFAR-10 training evolution, with mini-batch size 512. **Left:** Conditional entropy $\mathcal{H}(X^-|X)$ w.r.t. epoch. The maximal possible conditional entropy is indicated by a dotted line. **Right:** Linear classification with learned representations w.r.t. epoch.

This observation supports Lemmas 1 and 2 that the CL loss and its extensions optimize the encoder without considering the mutual information $I(X; X^-)$ and they will reach an optimum close to that of CCT when the data distribution does not clearly violate the uniform prior. In the case of $K = 4$, it is interesting to observe an obvious boost in performance, where CMC improves CL by around 2-3% while CCT improves CL by around 3-4%. This supports our analysis that using multiple positive samples is helpful to make the estimation of dissimilarity more accurate. Moreover, with multi-positive samples, CCT considers the dependency between positive samples, which enhances the robustness.

On the effect of conditional transport map: To understand the efficacy of the conditional transport maps, we show the evolution of conditional entropy $\mathcal{H}(X^-|X)$ and classification accuracy w.r.t. the training epoch as quantitative results and some qualitative illustrations. In each epoch, we calculate the conditional entropy with (11) on every mini-batch of size $M = 512$ (the last mini-batch will be ignored if the size is not 512) and take the average across the mini-batches. Figure 3 shows the evolution of $\mathcal{H}(X^-|X)$ during training, where we can observe $\mathcal{H}(X^-|X)$ is getting maximized as the encoder is getting optimized with these methods. As shown in Lemma 1, under the uniform data prior assumption, the optimization of CL and CCT encourages the encoder to maximize $\mathcal{H}(X^-|X)$. Moreover, shown in Lemma 2, the CL loss asymptotically maximizes $\mathcal{H}(X^-|X)$ with infinite samples. Here the gap between existing CL methods and CCT shows, with finite negative samples, directly optimizing CCT can be superior. It is also interesting to observe that in the case with multiple positive samples, the gap between CCT and CMC is quite large in terms of the conditional entropy, which illustrates the efficacy of conditional transport maps. In addition to the conditional entropy, we present the linear classification results with learned representations every 10 epochs, as shown in Figure 3. We can observe CCT consistently provide better performance than the other methods at the same epoch, indicating the sample efficiency of CCT. On CIFAR-100 and STL-10, the observations in Appendix C are similar.

As a qualitative verification, we randomly take a query from a mini-batch, and illustrate its positive and negative samples with the conditional transport probability in Figure 4. As shown, given this dog image as a query, the positive sample with the largest weight contains partial dog information, indicating the encoder to focus on texture information; the negatives with larger weights are more related to the dog category, which encourages the encoder to focus on distinguishing these “hard” samples. In sum, the weights learned by CCT is more interpretable than conventional CL.

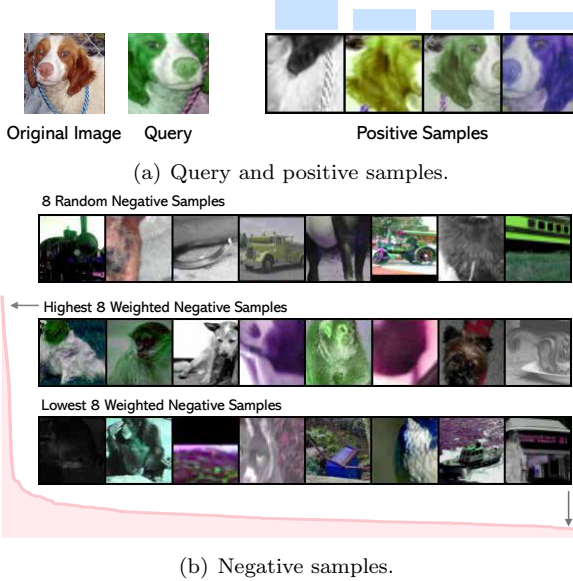


Figure 4: Illustration of positive/negative samples and their corresponding weights. (a) For a query augmented from the original dog image, 4 positive samples are shown, with their weights visualized as the blue distribution. (b) The weights for negative samples are visualized as the red distribution. To compare with the 8 random negative samples in the 1st row, we show 8 negative samples with the highest and lowest weights in the 2nd and 3rd row, respectively.

Table 2: The classification accuracy (%) of different contrastive objectives on class-imbalanced datasets. ‘‘Linear’’ and ‘‘Exponential’’ indicate the number of samples in each class are chosen by following a linear rule or an exponential rule, respectively. The performance drops compared with the performance in Table 1 are shown next to each result.

Imbalance	Linear		Exponential	
	Dataset	CIFAR-10	CIFAR-100	CIFAR-10
CL	79.88 _{3.59↓}	52.29 _{3.57↓}	71.74 _{11.73↓}	43.29 _{12.57↓}
AU-CL	80.25 _{3.14↓}	52.74 _{2.57↓}	71.62 _{11.76↓}	44.38 _{10.93↓}
HN-CL	80.51 _{3.15↓}	52.72 _{3.14↓}	72.74 _{10.93↓}	45.13 _{10.73↓}
CCT ($K = 1$)	80.46 _{3.27↓}	54.12 _{2.40↓}	73.02 _{10.71↓}	46.59 _{9.93↓}
CMC ($K = 4$)	82.20 _{3.34↓}	55.38 _{3.26↓}	74.77 _{10.77↓}	48.87 _{9.77↓}
CCT ($K = 4$)	83.62 _{2.92↓}	56.91 _{2.50↓}	75.89 _{10.65↓}	50.17 _{9.24↓}

5.2 Classification on Class-Imbalanced Datasets

As analyzed before, when the data distribution coincides with the uniform prior assumption, CL loss and CCT loss optimize the encoder to reach close optima. Here we create two class-imbalanced datasets with CIFAR-10 and CIFAR-100 to verify if CCT shows better robustness when this uniform prior assumption is violated. The imbalanced dataset is created by randomly sampling a certain number of samples from each class with a ‘‘linear’’ or ‘‘exponential’’ rule (Kim et al., 2020). Specifically, given a dataset with C classes, for class $l \in \{1, 2, \dots, C\}$, we randomly take samples with a proportion $\lfloor \frac{l}{C} \rfloor$ for ‘‘linear’’ rule and with a proportion $\exp(\lfloor \frac{l}{C} \rfloor)$ for ‘‘exponential’’ rule. Once the dataset is sampled, it is fixed during training. For evaluation we keep the same validation/testing datasets used in the standard case.

Summarized in Table 2 are the results on class-imbalanced datasets, which show all the methods have a performance drop compared to the results in Table 1. It is clear that CCT has the least performance decline in most cases. Especially, when $K = 4$, the transport map shows better performance robustness due to the characteristic of multiple contrastively reweighted positive samples. For example, in the ‘‘exponential’’ setting of CIFAR-100, The performance of CL and HN-CL drops 12.57% and 10.73%, respectively, while CCT ($K = 4$) drops 9.24%. It is also interesting to observe HN-CL is relatively better among the baseline methods. According to Robinson et al. (2021), in HN-CL the negative samples are sampled according to the ‘‘hardness’’ *w.r.t.* the query samples but not uniformly sampled. Its loss could converge to CCT ($K = 1$) with infinite negative samples. This performance gap indicates that directly optimizing the CCT loss could be superior when we have a limited number of samples. With this class-imbalanced datasets, we provide the empirical support to

Table 3: The top-1 classification accuracy (%) of different contrastive objectives with MoCo-v2 framework on the ImageNet dataset. All methods apply MoCo-v2 with ResNet50. The results from paper or Github page are marked by \star .

Methods	ImageNet-100	ImageNet-1K
CL	77.54 \star	67.50 \star
AU-CL	77.66 \star	67.69 \star
HN-CL	76.34	67.41
CMC ($K = 1$)	75.80 \star	66.20 \star
CCT ($K = 1$)	79.40	68.40
CMC ($K = 4$)	78.84	69.45
CCT ($K = 4$)	80.46	70.35

our analysis: The independent and uniform sampling of positive and negative is based on a uniform assumption of data distribution. When this assumption is violated, modeling the dependency between samples or specific sampling mechanism becomes necessary for contrastive representation learning.

5.3 Linear Classification on Large-scale Datasets

For large-scale experiments, following the convention, we adapt all methods into the MoCo-v2 framework and pre-train a ResNet50 encoder in 200 epochs with mini-batch size 128/256 on ImageNet-100/ImageNet-1k. Considering the setting of CMC is not readily compatible with the MoCo-v2 framework, we also report the results from [Tian et al. \(2019; 2020a\)](#) for two color channels of one sample (approximately considered as $K = 1$) as reference. Table 3 summarizes the results of linear classification on these two large-scale datasets. Similar to the case on small-scale datasets, CCT consistently shows better performance than the baseline methods and improves the baselines at least by 1.74% on ImageNet-100 and 0.71% on ImageNet-1K. In MoCo-v2, with multiple positive samples, CCT improves the baseline methods by 2.92% on ImageNet-100 and 2.75% on ImageNet-1K. It is worth highlighting that the improvement of CCT is more significant on these large-scale datasets, where the data distribution could be much more diverse compared to these small-scale ones. This is not surprising, as according to our theoretical analysis, CCT’s conditional transport map between samples enhances the effectiveness of the encoder’s optimization.

5.4 Object Detection and Segmentation

A main goal of unsupervised learning is to capture sufficiently general and transferrable representations. Besides the linear classification evaluation, we also transfer the pre-trained contrastive models as the initialization for fine-tuning in downstream tasks, such as object detection and segmentation. To evaluate the transfer ability of learned features, following the protocols in previous works ([Tian et al., 2019](#); [He et al., 2020](#); [Chen et al., 2020c](#); [Wang & Isola, 2020](#)), we use the pretrained ResNet50 on ImageNet-1K for object detection and segmentation task on Pascal VOC ([Everingham et al., 2010](#)) and COCO ([Lin et al., 2014](#)) by using detectron2 ([Wu et al., 2019](#)). The experimental setting details are shown in Section B.2 and kept the same as [He et al. \(2020\)](#) and [Chen et al. \(2020c\)](#). The test AP, AP₅₀, and AP₇₅ of bounding boxes in object detection and test AP, AP₅₀, and AP₇₅ of masks in segmentation are reported in Table 4. We can observe that the performances of CCT are consistently better than that of other contrastive objectives. For example, compared to CL, the APs on Pascal VOC detection has been improved by 0.91%. In segmentation tasks, the AP is improved by 0.31%.

Table 4: Results of transferring features to object detection and segmentation task on Pascal VOC, with the pre-trained MoCo-v2 ResNet50 on ImageNet-1k. The results of CL loss on Pascal VOC are from their papers and online Github pages.

Task	Object Detection						Object Segmentation		
	Pascal VOC			COCO			COCO		
Dataset	AP	AP ₅₀	AP ₇₅	AP	AP ₅₀	AP ₇₅	AP	AP ₅₀	AP ₇₅
Loss									
CL	57.00	82.40	63.60	40.90	60.53	44.30	35.73	57.29	38.20
AU-CL	57.24	82.49	63.83	41.01	60.68	44.40	35.56	57.38	37.93
CCT ($K = 1$)	57.75	82.76	64.23	41.08	60.80	44.84	35.74	57.50	38.07
CCT ($K = 4$)	57.91	82.83	64.85	41.50	61.11	45.30	36.08	57.95	38.68

6 Conclusion

In this paper, we rethink the limitation of conventional contrastive learning (CL) methods that form the contrastive loss by randomly selecting positive and negative samples for a query. We introduce a novel contrastive conditional transport (CCT) loss that constructs for a random query two contradicting conditional transport maps, which model the importance of a positive sample and that of a negative sample, respectively, to the query. To form the contrastive loss, CCT combines the independent and random sampling convention with the practice of contrastively reweighing both positive and negative samples according to their distances to the query. Our theoretical analysis and empirical results show that optimizing the CCT loss helps align positive samples with the query and reduce the mutual information between the negative samples and query. Extensive experiments on small, large-scale, and imbalanced datasets consistently demonstrate the superiority and robustness of CCT over the state-of-the-art methods in contrastive representation learning and related downstream tasks.

References

Bachman, P., Hjelm, R. D., and Buchwalter, W. Learning representations by maximizing mutual information across views. In *Advances in Neural Information Processing Systems*, 2019.

Bengio, Y., Courville, A., and Vincent, P. Representation learning: A review and new perspectives. *IEEE transactions on pattern analysis and machine intelligence*, 35(8):1798–1828, 2013.

Bose, A. J., Ling, H., and Cao, Y. Adversarial contrastive estimation. *arXiv preprint arXiv:1805.03642*, 2018.

Chen, T., Kornblith, S., Norouzi, M., and Hinton, G. A simple framework for contrastive learning of visual representations. *arXiv preprint arXiv:2002.05709*, 2020a.

Chen, T., Kornblith, S., Swersky, K., Norouzi, M., and Hinton, G. Big self-supervised models are strong semi-supervised learners. *arXiv preprint arXiv:2006.10029*, 2020b.

Chen, X., Fan, H., Girshick, R., and He, K. Improved baselines with momentum contrastive learning. *arXiv preprint arXiv:2003.04297*, 2020c.

Chen, X., Zhang, Y., Tsang, I., and Pan, Y. Learning robust node representations on graphs. *arXiv preprint arXiv:2008.11416*, 2020d.

Cherian, A. and Aeron, S. Representation learning via adversarially-contrastive optimal transport. *arXiv preprint arXiv:2007.05840*, 2020.

Chuang, C.-Y., Robinson, J., Lin, Y.-C., Torralba, A., and Jegelka, S. Debiased contrastive learning. *Advances in Neural Information Processing Systems*, 33, 2020.

Coates, A., Ng, A., and Lee, H. An analysis of single-layer networks in unsupervised feature learning. In *Proceedings of the fourteenth international conference on artificial intelligence and statistics*, pp. 215–223, 2011.

Davidson, T. R., Falorsi, L., De Cao, N., Kipf, T., and Tomczak, J. M. Hyperspherical variational auto-encoders. *arXiv preprint arXiv:1804.00891*, 2018.

Deng, J., Dong, W., Socher, R., Li, L.-J., Li, K., and Fei-Fei, L. Imagenet: A large-scale hierarchical image database. In *2009 IEEE conference on computer vision and pattern recognition*, pp. 248–255. Ieee, 2009.

Everingham, M., Van Gool, L., Williams, C. K., Winn, J., and Zisserman, A. The pascal visual object classes (voc) challenge. *International journal of computer vision*, 88(2):303–338, 2010.

Fang, H. and Xie, P. Cert: Contrastive self-supervised learning for language understanding. *arXiv preprint arXiv:2005.12766*, 2020.

Giorgi, J. M., Nitski, O., Bader, G. D., and Wang, B. Declutr: Deep contrastive learning for unsupervised textual representations. *ArXiv*, abs/2006.03659, 2020.

Goyal, P., Dollár, P., Girshick, R., Noordhuis, P., Wesolowski, L., Kyrola, A., Tulloch, A., Jia, Y., and He, K. Accurate, large minibatch sgd: Training imagenet in 1 hour. *arXiv preprint arXiv:1706.02677*, 2017.

Gutmann, M. and Hyvärinen, A. Noise-contrastive estimation: A new estimation principle for unnormalized statistical models. In *Proceedings of the Thirteenth International Conference on Artificial Intelligence and Statistics*, pp. 297–304, 2010.

Hassani, K. and Khasahmadi, A. H. Contrastive multi-view representation learning on graphs. In *International Conference on Machine Learning*, pp. 3451–3461, 2020.

He, K., Zhang, X., Ren, S., and Sun, J. Deep residual learning for image recognition. In *2016 IEEE Conference on Computer Vision and Pattern Recognition (CVPR)*, pp. 770–778, 2016. doi: 10.1109/CVPR.2016.90.

He, K., Gkioxari, G., Dollár, P., and Girshick, R. Mask r-cnn. In *Proceedings of the IEEE international conference on computer vision*, pp. 2961–2969, 2017.

He, K., Fan, H., Wu, Y., Xie, S., and Girshick, R. Momentum contrast for unsupervised visual representation learning. In *Proceedings of the IEEE/CVF Conference on Computer Vision and Pattern Recognition (CVPR)*, June 2020.

Hénaff, O. J., Razavi, A., Doersch, C., Eslami, S., and Oord, A. v. d. Data-efficient image recognition with contrastive predictive coding. *arXiv preprint arXiv:1905.09272*, 2019.

Hinton, G. E. Learning multiple layers of representation. *Trends in cognitive sciences*, 11(10):428–434, 2007.

Hinton, G. E. and Salakhutdinov, R. R. Reducing the dimensionality of data with neural networks. *science*, 313(5786):504–507, 2006.

Hjelm, R. D., Fedorov, A., Lavoie-Marchildon, S., Grewal, K., Bachman, P., Trischler, A., and Bengio, Y. Learning deep representations by mutual information estimation and maximization. In *International Conference on Learning Representations*, 2018.

Kalantidis, Y., Sariyildiz, M. B., Pion, N., Weinzaepfel, P., and Larlus, D. Hard negative mixing for contrastive learning. *arXiv preprint arXiv:2010.01028*, 2(6), 2020.

Khosla, P., Teterwak, P., Wang, C., Sarna, A., Tian, Y., Isola, P., Maschinot, A., Liu, C., and Krishnan, D. Supervised contrastive learning. *Advances in Neural Information Processing Systems*, 33, 2020.

Kim, Y., Lee, Y., and Jeon, M. Imbalanced image classification with complement cross entropy. *arXiv preprint arXiv:2009.02189*, 2020.

Kingma, D. P. and Welling, M. Auto-encoding variational bayes. *International Conference on Learning Representations*, 2014.

Li, C., Li, X., Zhang, L., Peng, B., Zhou, M., and Gao, J. Self-supervised pre-training with hard examples improves visual representations. *arXiv preprint arXiv:2012.13493*, 2020.

Li, Y., Gu, C., Dullien, T., Vinyals, O., and Kohli, P. Graph matching networks for learning the similarity of graph structured objects. In *International Conference on Machine Learning*, pp. 3835–3845, 2019.

Lin, T.-Y., Maire, M., Belongie, S., Hays, J., Perona, P., Ramanan, D., Dollár, P., and Zitnick, C. L. Microsoft coco: Common objects in context. In *European conference on computer vision*, pp. 740–755. Springer, 2014.

Logeswaran, L. and Lee, H. An efficient framework for learning sentence representations. In *International Conference on Learning Representations*, 2018.

Misra, I. and Maaten, L. v. d. Self-supervised learning of pretext-invariant representations. In *Proceedings of the IEEE/CVF Conference on Computer Vision and Pattern Recognition*, pp. 6707–6717, 2020.

Oord, A. v. d., Li, Y., and Vinyals, O. Representation learning with contrastive predictive coding. *arXiv preprint arXiv:1807.03748*, 2018.

Poole, B., Ozair, S., van den Oord, A., Alemi, A. A., and Tucker, G. On variational lower bounds of mutual information. In *NeurIPS Workshop on Bayesian Deep Learning*, 2018.

Ren, S., He, K., Girshick, R., and Sun, J. Faster r-cnn: towards real-time object detection with region proposal networks. *IEEE transactions on pattern analysis and machine intelligence*, 39(6):1137–1149, 2016.

Robinson, J. D., Chuang, C.-Y., Sra, S., and Jegelka, S. Contrastive learning with hard negative samples. In *International Conference on Learning Representations*, 2021.

Saunshi, N., Plevrakis, O., Arora, S., Khodak, M., and Khandeparkar, H. A theoretical analysis of contrastive unsupervised representation learning. In Chaudhuri, K. and Salakhutdinov, R. (eds.), *Proceedings of the 36th International Conference on Machine Learning*, volume 97 of *Proceedings of Machine Learning Research*, pp. 5628–5637. PMLR, 09–15 Jun 2019a.

Saunshi, N., Plevrakis, O., Arora, S., Khodak, M., and Khandeparkar, H. A theoretical analysis of contrastive unsupervised representation learning. In *International Conference on Machine Learning*, pp. 5628–5637. PMLR, 2019b.

Srinivas, A., Laskin, M., and Abbeel, P. CURL: Contrastive unsupervised representations for reinforcement learning. In *International Conference on Machine Learning*, pp. 10360–10371, 2020.

Sun, F.-Y., Hoffmann, J., Verma, V., and Tang, J. InfoGraph: Unsupervised and semi-supervised graph-level representation learning via mutual information maximization. In *International Conference on Learning Representations*, 2020.

Sylvain, T., Petrini, L., and Hjelm, D. Locality and compositionality in zero-shot learning. In *International Conference on Learning Representations*, 2020.

Tian, Y., Krishnan, D., and Isola, P. Contrastive multiview coding. *arXiv preprint arXiv:1906.05849*, 2019.

Tian, Y., Krishnan, D., and Isola, P. Contrastive representation distillation. In *International Conference on Learning Representations*, 2020a.

Tian, Y., Sun, C., Poole, B., Krishnan, D., Schmid, C., and Isola, P. What makes for good views for contrastive learning. In *Advances in Neural Information Processing Systems*, 2020b.

Tipping, M. E. and Bishop, C. M. Probabilistic principal component analysis. *Journal of the Royal Statistical Society: Series B (Statistical Methodology)*, 61(3):611–622, 1999.

Tschannen, M., Djolonga, J., Rubenstein, P. K., Gelly, S., and Lucic, M. On mutual information maximization for representation learning. *arXiv preprint arXiv:1907.13625*, 2019.

van der Maaten, L. and Hinton, G. Visualizing data using t-sne. *Journal of Machine Learning Research*, 9(86):2579–2605, 2008.

Velickovic, P., Fedus, W., Hamilton, W. L., Liò, P., Bengio, Y., and Hjelm, R. D. Deep Graph Infomax. In *International Conference on Learning Representations*, 2019.

Wang, F., Xiang, X., Cheng, J., and Yuille, A. L. Normface: L2 hypersphere embedding for face verification. In *Proceedings of the 25th ACM international conference on Multimedia*, pp. 1041–1049, 2017.

Wang, T. and Isola, P. Understanding contrastive representation learning through alignment and uniformity on the hypersphere. In *International Conference on Machine Learning*, pp. 9929–9939. PMLR, 2020.

Wu, M., Mosse, M., Zhuang, C., Yamins, D., and Goodman, N. Conditional negative sampling for contrastive learning of visual representations. In *International Conference on Learning Representations*, 2021.

Wu, Y., Kirillov, A., Massa, F., Lo, W.-Y., and Girshick, R. Detectron2. <https://github.com/facebookresearch/detectron2>, 2019.

Wu, Z., Xiong, Y., Stella, X. Y., and Lin, D. Unsupervised feature learning via non-parametric instance discrimination. In *Proceedings of the IEEE Conference on Computer Vision and Pattern Recognition*, 2018.

Zheng, H. and Zhou, M. Comparing probability distributions with conditional transport. *arXiv preprint arXiv:2012.14100*, 2020.

Contrastive Conditional Transport for Representation Learning: Appendix

A Proofs and Detailed Derivation

Proof of Property 1. By definition, the point-to-point transport cost $c(\mathbf{z}_1, \mathbf{z}_2)$ is always non-negative. Without loss of generality, we define it with the Euclidean distance. When (10) is true, the expected cost of transporting between a pair of positive samples, as defined as \mathcal{C}^+ in (4), will reach its minimum at 0. When (10) is not true, by definition we will have $\mathcal{C}^+ > 0$, i.e., $\mathcal{C}^+ = 0$ is possible only if (10) is true. \square

Proof of Lemma 1. Denoting

$$Z(\mathbf{x}) = \int e^{-d(f_{\theta}(\mathbf{x}), f_{\theta}(\mathbf{x}^-))} p(\mathbf{x}^-) d\mathbf{x}^-,$$

we have

$$-\ln \pi_{\theta}^-(\mathbf{x}^- | \mathbf{x}) = d(f_{\theta}(\mathbf{x}), f_{\theta}(\mathbf{x}^-)) - \ln p(\mathbf{x}^-) + \ln Z(\mathbf{x}).$$

Thus we have

$$\begin{aligned} \mathcal{C}^- &= \mathbb{E}_{\mathbf{x} \sim p(\mathbf{x})} \mathbb{E}_{\mathbf{x}^- \sim \pi_{\theta}^-(\cdot | \mathbf{x})} [-\ln \pi_{\theta}^-(\mathbf{x}^- | \mathbf{x}) + \ln p(\mathbf{x}^-) - \ln Z(\mathbf{x})] \\ &= \mathcal{H}(X^- | X) + C_1 + C_2 \end{aligned} \quad (13)$$

where $C_1 = \mathbb{E}_{\mathbf{x} \sim p(\mathbf{x})} \mathbb{E}_{\mathbf{x}^- \sim \pi_{\theta}^-(\cdot | \mathbf{x})} [\ln p(\mathbf{x}^-)]$ and $C_2 = -\mathbb{E}_{\mathbf{x} \sim p(\mathbf{x})} \ln Z(\mathbf{x})$. Under the assumption of a uniform prior on $p(\mathbf{x})$, C_1 becomes a term that is not related to θ . Under the assumption of a uniform prior on $p(\mathbf{z})$, where $\mathbf{z} = f_{\theta}(\mathbf{x})$, we have

$$\begin{aligned} Z(\mathbf{x}) &= \mathbb{E}_{\mathbf{x}^- \sim p(\mathbf{x})} [e^{-d(f_{\theta}(\mathbf{x}), f_{\theta}(\mathbf{x}^-))}] \\ &= \mathbb{E}_{\mathbf{z}^- \sim p(\mathbf{z})} [e^{-(\mathbf{z}^- - \mathbf{z})^T (\mathbf{z}^- - \mathbf{z})}] \\ &\propto \int e^{-(\mathbf{z}^- - \mathbf{z})^T (\mathbf{z}^- - \mathbf{z})} d\mathbf{z}^- \\ &= \sqrt{\pi}, \end{aligned} \quad (14)$$

which is also not related to θ . Therefore, under the uniform prior assumption on both $p(\mathbf{x})$ and $p(\mathbf{z})$, maximizing \mathcal{C}^- is the same as maximizing \mathcal{H} . \square

Proof of Lemma 2. The CL loss can be decomposed as an expected dissimilarity term and a log-sum-exp term:

$$\begin{aligned} \mathcal{L}_{\text{CL}} &:= \mathbb{E}_{(\mathbf{x}, \mathbf{x}^+, \mathbf{x}_{1:M}^-)} \left[-\ln \frac{e^{f_{\theta}(\mathbf{x})^T f_{\theta}(\mathbf{x}^+)/\tau}}{e^{f_{\theta}(\mathbf{x})^T f_{\theta}(\mathbf{x}^+)/\tau} + \sum_i e^{f_{\theta}(\mathbf{x}_i^-)^T f_{\theta}(\mathbf{x})/\tau}} \right] \\ &= \mathbb{E}_{(\mathbf{x}, \mathbf{x}^+)} \left[-\frac{1}{\tau} f_{\theta}(\mathbf{x})^T f_{\theta}(\mathbf{x}^+) \right] + \mathbb{E}_{(\mathbf{x}, \mathbf{x}^+, \mathbf{x}_{1:M}^-)} \left[\ln \left(e^{f_{\theta}(\mathbf{x})^T f_{\theta}(\mathbf{x}^+)/\tau} + \sum_{i=1}^M e^{f_{\theta}(\mathbf{x}_i^-)^T f_{\theta}(\mathbf{x})/\tau} \right) \right], \end{aligned}$$

where the positive sample \mathbf{x}^+ is independent of \mathbf{x} given \mathbf{x}_0 and the negative samples \mathbf{x}_i^- are independent of \mathbf{x} . As the number of negative samples goes to infinity, following Wang & Isola (2020), the normalized CL loss is decomposed into the sum of the align loss, which describes the contribution of the positive samples, and the uniform loss, which describes the contribution of the negative samples:

$$\lim_{M \rightarrow \infty} \mathcal{L}_{\text{CL}} - \ln M = \underbrace{\mathbb{E}_{(\mathbf{x}, \mathbf{x}^+)} \left[-\frac{1}{\tau} f_{\theta}(\mathbf{x})^T f_{\theta}(\mathbf{x}^+) \right]}_{\text{contribution of positive samples}} + \underbrace{\mathbb{E}_{\mathbf{x} \sim p(\mathbf{x})} \left[\ln \mathbb{E}_{\mathbf{x}^- \sim p(\mathbf{x}^-)} e^{f_{\theta}(\mathbf{x}^-)^T f_{\theta}(\mathbf{x})/\tau} \right]}_{\text{contribution of negative samples}}$$

With importance sampling, the second term in the RHS of the above equation can be further derived into:

$$\begin{aligned} &\mathbb{E}_{\mathbf{x} \sim p(\mathbf{x})} \left[\ln \mathbb{E}_{\mathbf{x}^- \sim p(\mathbf{x}^-)} e^{f_{\theta}(\mathbf{x}^-)^T f_{\theta}(\mathbf{x})/\tau} \right] \\ &= \mathbb{E}_{\mathbf{x} \sim p(\mathbf{x})} \left[\ln \mathbb{E}_{\mathbf{x}^- \sim \pi_{\theta}(\mathbf{x}^- | \mathbf{x})} \left[e^{f_{\theta}(\mathbf{x}^-)^T f_{\theta}(\mathbf{x})/\tau} \frac{p(\mathbf{x}^-)}{\pi_{\theta}(\mathbf{x}^- | \mathbf{x})} \right] \right] \end{aligned}$$

Apply the Jensen inequality, the second term is decomposed into the negative transport plus a log density ratio:

$$\begin{aligned}
& \mathbb{E}_{\mathbf{x} \sim p(\mathbf{x})} \left[\ln \mathbb{E}_{\mathbf{x}^- \sim p(\mathbf{x}^-)} e^{f_{\boldsymbol{\theta}}(\mathbf{x}^-)^\top f_{\boldsymbol{\theta}}(\mathbf{x})/\tau} \right] \\
& \geq \mathbb{E}_{\mathbf{x} \sim p(\mathbf{x})} \left[\mathbb{E}_{\mathbf{x}^- \sim \pi_{\boldsymbol{\theta}}(\mathbf{x}^- | \mathbf{x})} [f_{\boldsymbol{\theta}}(\mathbf{x}^-)^\top f_{\boldsymbol{\theta}}(\mathbf{x})/\tau] \right] + \mathbb{E}_{\mathbf{x} \sim p(\mathbf{x})} \left[\mathbb{E}_{\mathbf{x}^- \sim \pi_{\boldsymbol{\theta}}(\mathbf{x}^- | \mathbf{x})} \left[\ln \frac{p(\mathbf{x}^-)}{\pi_{\boldsymbol{\theta}}(\mathbf{x}^- | \mathbf{x})} \right] \right] \\
& = \mathbb{E}_{\mathbf{x} \sim p(\mathbf{x})} \left[\mathbb{E}_{\mathbf{x}^- \sim \pi_{\boldsymbol{\theta}}(\mathbf{x}^- | \mathbf{x})} [f_{\boldsymbol{\theta}}(\mathbf{x}^-)^\top f_{\boldsymbol{\theta}}(\mathbf{x})/\tau] \right] - I(X; X^-)
\end{aligned}$$

Defining the point-to-point cost function between two unit-norm vectors as $c(\mathbf{z}_1, \mathbf{z}_2) = -\mathbf{z}_1^\top \mathbf{z}_2$ (same as the Euclidean cost since $\|\mathbf{z}_1 - \mathbf{z}_2\|_2^2/2 = 1 - \mathbf{z}_1^\top \mathbf{z}_2$), we have

$$\begin{aligned}
& \mathbb{E}_{\mathbf{x} \sim p(\mathbf{x})} \left[\ln \mathbb{E}_{\mathbf{x}^- \sim p(\mathbf{x})} e^{f_{\boldsymbol{\theta}}(\mathbf{x}^-)^\top f_{\boldsymbol{\theta}}(\mathbf{x})/\tau} \right] + I(X; X^-) \\
& \geq \mathbb{E}_{\mathbf{x} \sim p(\mathbf{x})} \left[\mathbb{E}_{\mathbf{x}^- \sim \pi_{\boldsymbol{\theta}}(\mathbf{x}^- | \mathbf{x})} [f_{\boldsymbol{\theta}}(\mathbf{x}^-)^\top f_{\boldsymbol{\theta}}(\mathbf{x})/\tau] \right] \\
& = - \mathbb{E}_{\mathbf{x} \sim p(\mathbf{x})} \left[\mathbb{E}_{\mathbf{x}^- \sim \pi_{\boldsymbol{\theta}}(\mathbf{x}^- | \mathbf{x})} [c(f_{\boldsymbol{\theta}}(\mathbf{x}^-), f_{\boldsymbol{\theta}}(\mathbf{x}))/\tau] \right] \\
& = -\mathcal{C}^-.
\end{aligned}$$

This concludes the relation between the contribution of negative samples in CL and that in CCT. \square

B Experiment Details

On small-scale datasets, all experiments are conducted on a single GPU, including NVIDIA 1080 Ti and RTX 3090; on large-scale datasets, all experiments are done on 8 Tesla-V100-32G GPUs.

B.1 Small-scale Datasets: CIFAR-10, CIFAR-100 and STL-10

For experiments on CIFAR-10, CIFAR-100, and STL-10, we use the following configurations:

- **Data Augmentation:** We strictly follow the standard data augmentations to construct positive and negative samples introduced in prior works in contrastive learning (Wu et al., 2018; Tian et al., 2019; Hjelm et al., 2018; Bachman et al., 2019; Chuang et al., 2020; He et al., 2020; Wang & Isola, 2020). The augmentations include image resizing, random cropping, flipping, color jittering, and gray-scale conversion. We provide a Pytorch-style augmentation code in Algorithm 1, which is exactly the same as the one used in Wang & Isola (2020).

Algorithm 1 PyTorch-like Augmentation Code on CIFAR-10, CIFAR-100 and STL-10

```
import torchvision.transforms as transforms

# CIFAR-10 Transformation
def transform_cifar10():
    return transforms.Compose([
        transforms.RandomResizedCrop(32, scale=(0.2, 1)),
        transforms.RandomHorizontalFlip(), # by default p=0.5
        transforms.ColorJitter(0.4, 0.4, 0.4, 0.4),
        transforms.RandomGrayscale(p=0.2),
        transforms.ToTensor(), # normalize to value in [0,1]
        transforms.Normalize(
            (0.4914, 0.4822, 0.4465),
            (0.2023, 0.1994, 0.2010),
        )
    ])

# CIFAR-100 Transformation
def transform_cifar100():
    return transforms.Compose([
        transforms.RandomResizedCrop(32, scale=(0.2, 1)),
        transforms.RandomHorizontalFlip(), # by default p=0.5
        transforms.ColorJitter(0.4, 0.4, 0.4, 0.4),
        transforms.RandomGrayscale(p=0.2),
        transforms.ToTensor(), # normalize to value in [0,1]
        transforms.Normalize(
            (0.5071, 0.4867, 0.4408),
            (0.2675, 0.2565, 0.2761),
        )
    ])

# STL-10 Transformation
def transform_stl10():
    return transforms.Compose([
        transforms.RandomResizedCrop(64, scale=(0.08, 1)),
        transforms.RandomHorizontalFlip(), # by default p=0.5
        transforms.ColorJitter(0.4, 0.4, 0.4, 0.4),
        transforms.RandomGrayscale(p=0.2),
        transforms.ToTensor(), # normalize to value in [0,1]
        transforms.Normalize(
            (0.4409, 0.4279, 0.3868),
            (0.2683, 0.2610, 0.2687),
        )
    ])
```

- **Feature Encoder:** Following the experiments in Wang & Isola (2020), we use an AlexNet-based encoder as the feature encoder for these three datasets. The encoder architectures are the same as those used in the corresponding experiments in Tian et al. (2019) and Wang & Isola (2020). Moreover, we also follow the setups in Robinson et al. (2021) and test the performance of CCT with a ResNet50 encoder (results are shown in Table 6).
- **Model Optimization:** We apply the mini-batch SGD with 0.9 momentum and 1e-4 weight decay. The learning rate is linearly scaled as 0.12 per 256 batch size (Goyal et al., 2017). The optimization is done over 200 epochs, and the learning rate is decayed by a factor of 0.1 at epoch 155, 170, and 185.

Table 5: The 100 randomly selected classes from ImageNet forms the ImageNet-100 dataset. These classes are the same as (Wang & Isola, 2020; Tian et al., 2019).

ImageNet-100 Classes									
n02869837	n01749939	n02488291	n02107142	n13037406	n02091831	n04517823	n04589890	n03062245	n01773797
n01735189	n07831146	n07753275	n03085013	n04485082	n02105505	n01983481	n02788148	n03530642	n04435653
n02086910	n02859443	n13040303	n03594734	n02085620	n02099849	n01558993	n04493381	n02109047	n04111531
n02877765	n04429376	n02009229	n01978455	n02106550	n01820546	n01692333	n07714571	n02974003	n02114855
n03785016	n03764736	n03775546	n02087046	n07836838	n04099969	n04592741	n03891251	n02701002	n03379051
n02259212	n07715103	n03947888	n04026417	n02326432	n03637318	n01980166	n02113799	n02086240	n03903868
n02483362	n04127249	n02089973	n03017168	n02093428	n02804414	n02396427	n04418357	n02172182	n01729322
n02113978	n03787032	n02089867	n02119022	n03777754	n04238763	n02231487	n03032252	n02138441	n02104029
n03837869	n03494278	n04136333	n03794056	n03492542	n02018207	n04067472	n03930630	n03584829	n02123045
n04229816	n02100583	n03642806	n04336792	n03259280	n02116738	n02108089	n03424325	n01855672	n02090622

- **Parameter Setup:** On CIFAR-10, CIFAR-100, and STL-10, we follow Wang & Isola (2020) to set the training batch size as $M = 768$ for baselines. The hyper-parameters of CL, AU-CL¹, and HN-CL² are set according to the original paper or online codes. Specifically, the temperature parameter of CL is $\tau = 0.19$, the hyper-parameters of AU-CL are $t = 2.0, \tau = 0.19$, and the hyper-parameter of HN-CL are $\tau = 0.5, \beta = 1.0$.³ For CMC and CCT with multiple positives, the positive sampling size is $K = 4$. To make sure the performance is not improved by using more samples, the training batch size is set as $M = 128$. For CCT, in both single and multi-positive sample settings, we set $t^+ = 1.0$ for all small-scale datasets. As for t^- , for CCT ($K = 1$), t^- is 2.0, 3.0, and 3.0 on CIFAR-10, CIFAR100, and STL-10, respectively. For CCT ($K = 4$), t^- is 0.9, 2.0, and 2.0 on CIFAR-10, CIFAR100, and STL-10, respectively. For further ablation studies, we test t^+ and t^- with the search in the range of $[0.5, 0.7, 0.9, 1.0, 2.0, 3.0]$, and we test all the methods with several mini-batch sizes $M \in \{64, 128, 256, 512, 768\}$.
- **Evaluation:** The feature encoder is trained with the default built-in training set of the datasets. In the evaluation, the feature encoder is frozen, and a linear classifier is trained and tested on the default training set and validation set of each dataset, respectively. Following Wang & Isola (2020), we train the linear classifier with Adam optimizer over 100 epochs, with $\beta_1 = 0.5$, $\beta_2 = 0.999$, $\epsilon = 10^{-8}$, and 128 as the batch size. The initial learning rate is 0.001 and decayed by a factor of 0.2 at epoch 60 and epoch 80. Extracted features from “fc7” are employed for the evaluation.

B.2 Large-scale datasets: ImageNet-100 and ImageNet-1K

For large-scale datasets, the Imagenet-1K is the standard ImageNet dataset that has about 1.28 million images of 1000 classes. The ImageNet-100 contains randomly selected 100 classes from the standard ImageNet-1K dataset, and the classes used here are the same with Tian et al. (2019) and Wang & Isola (2020), listed in Table 5. We follow the standard settings in these works and describe the experiment configurations as follows:

- **Data Augmentation:** Following Tian et al. (2019; 2020b); Wang & Isola (2020); Chuang et al. (2020); He et al. (2020); Chen et al. (2020c), the data augmentations are the same as the standard protocol, including resizing, 1x image cropping, horizontal flipping, color jittering, and gray-scale conversion with specific probability. The full augmentation combination is shown in Algorithm 2.
- **Feature Encoder:** On these two datasets, we apply the MoCo-v2 framework (Chen et al., 2020c), where the ResNet50 (He et al., 2016) is a commonly chosen feature encoder architecture. The output dimension of the encoder is set as 128.
- **Model Optimization:** Following the standard setting in He et al. (2020); Chen et al. (2020c); Wang & Isola (2020), the training mini-batch size is set as 128 on ImageNet-100 and 256 on ImageNet-1K. We use a mini-batch stochastic gradient descent (SGD) optimizer with 0.9 momentum and 1e-4 weight decay. The total number of training epochs is set as 200. The learning rate is initialized as 0.03, decayed by a cosine scheduler for MoCo-V2 at epoch 120 and epoch 160. In all experiments, the momentum of updating the offline encoder is 0.999.

¹https://github.com/SsnL/align_uniform

²<https://github.com/joshr17/HCL>

³Please refer to the original paper for the specific meanings of the hyper-parameter in baselines.

Algorithm 2 PyTorch-like Augmentation Code on ImageNet-100 and ImageNet-1K

```

import torchvision.transforms as transforms
# ImageNet-100 and ImageNet-1K Transformation
# MoCo v2's aug: similar to SimCLR https://arxiv.org/abs/2002.05709
def transform_imagenet():
    return transforms.Compose([
        transforms.RandomResizedCrop(224, scale=(0.2, 1.)),
        transforms.RandomApply([transforms.ColorJitter(0.4, 0.4, 0.4, 0.1)
                               , p=0.8),
        transforms.RandomGrayscale(p=0.2),
        transforms.RandomApply([moco.loader.GaussianBlur([.1, 2.])], p=0.5),
        transforms.RandomHorizontalFlip(),
        transforms.ToTensor(),
        transforms.Normalize(mean=[0.485, 0.456, 0.406],
                           std=[0.229, 0.224, 0.225])
    ])

```

- **Parameter Setup:** On ImageNet-100 and ImageNet-1K, for all methods, the queue size for negative sampling is 65,536. The training batch size is 128 on ImageNet-100 and 256 on ImageNet. For CCT, we train with two positive sampling sizes $K = 1$ and $K = 4$ and the parameters in the conditional weight metric are respectively set as $t^+ = 1.0$, $t^- = 2.0$. For baselines, according to their papers and Github pages (Tian et al., 2019; Wang & Isola, 2020; Robinson et al., 2021), the temperature parameter of CL is $\tau = 0.2$, the hyper-parameters of AU-CL are $t = 3.0$, $\tau = 0.2$, and the hyper-parameters of HN-CL are $\tau = 0.5$, $\beta = 1.0$. CMC ($K = 1$) reported in the main paper is trained with 240 epochs and with its own augmentation methods (Tian et al., 2019). For CMC ($K = 4$), the temperature is set $\tau = 0.07$ according to the setting in Tian et al. (2019) and the loss is calculated with Equation (8) in the paper, which requires more GPU resources than 8 Tesla-V100-32G GPUs with the setting on ImageNet-1K.
- **Linear Classification Evaluation:** Following the standard linear classification evaluation (He et al., 2020; Chen et al., 2020c; Wang & Isola, 2020), the pre-trained feature encoders are fixed, and a linear classifier added on top is trained on the train split and test on the validation split. The linear classifier is trained with SGD over 100 epochs, with the momentum as 0.9, the mini-batch size as 256, and the learning rate as 30.0, decayed by a factor of 0.1 at epoch 60 and epoch 80.
- **Feature Transferring Evaluation (Detection and Segmentation):** The pre-trained models are transferred to various tasks including PASCAL VOC⁴ and COCO⁵ datasets. Strictly following the same setting in He et al. (2020), for the detection on Pascal VOC, a Faster R-CNN (Ren et al., 2016) with an R50-C4 backbone is first fine-tuned end-to-end on the VOC 07+12 trainval set and then evaluated on the VOC 07 test set with the COCO suite of metrics (Lin et al., 2014). The image scale is [480, 800] pixels during training and 800 at inference. For the detection and segmentation on COCO dataset, a Mask R-CNN (He et al., 2017) with C4 backbone (1x schedule) is applied for the end-to-end fine-tuning. The model is tuned on the train2017 set and evaluate on val2017 set, where the image scale is in [640, 800] pixels during training and is 800 in the inference.
- **Estimation of $\hat{\pi}_{\theta}^-$ with MoCo-v2:** Following the strategy in Wang & Isola (2020), we estimate $\hat{\pi}_{\theta}^-$ with not only the transport between queries and keys, but also with the transport between queries. Specifically, at each iteration, let M be the mini-batch size, N be the queue size, $\{f_{q_i}\}_{i=1}^M$ be the query features, and $\{f_{k_j}\}_{j=1}^N$ be the key features. The transport map is calculated as:

$$\hat{\pi}_{\theta}^-(\cdot | f_{q_i}) = \frac{e^{-d_t^-(\cdot, f_{q_i})}}{\sum_{j=1}^N e^{-d_t^-(f_{k_j}, f_{q_i})} + \sum_{j \neq i} e^{-d_t^-(f_{q_j}, f_{q_i})}}$$

To be clear, the Pytorch-like pseudo-code is provided in Algorithm 3. In MoCo-v2 framework, as the keys are produced from the momentum encoder, this estimation could help the main encoder get involved with the gradient from the transport map, which is consistent with the formulation in Section 3.3.

⁴<http://host.robots.ox.ac.uk/pascal/VOC/index.html>
⁵<https://cocodataset.org/#download>

Algorithm 3 PyTorch-like style pseudo-code of CCT with MoCo-v2 at each iteration.

```

#####
# Inputs #####
# t_pos, t_neg: hyper-parameters in CCT
# m: momentum
# im_list=[B0, B2, ..., BK] list of mini-batches of length (K+1)
# B: mini-batches (Mx3x224x224), M denotes batch_size
# encoder_q: main encoder; encoder_k: momentum encoder
# queue: dictionary as a queue of N features of keys (dxN); d denotes the feature dimension

##### compute the embeddings of all samples #####
q_list = [encoder_q(im) for im in im_list] # a list of (K+1) queries q: M x d
k_list = [encoder_k(im) for im in im_list]
stacked_k = torch.stack(k_list, dim=0) # keys k: (K+1) x M x d

##### compute the loss #####
CCT_loss_pos, CCT_loss_neg = 0.0, 0.0
for k in range(len(im_list)): #load a mini-batch with M samples as queries
    q = q_list[k]
    mask = list(range(len(im_list)))
    mask.pop(k) # the rest mini-batches are used as positive and negative samples

    ##### compute the positive transport #####
    # calculate the cost of transporting positive samples: M x K
    cost_for_pos = (q - stacked_k[mask]).norm(p=2, dim=-1).pow(2).transpose(1, 0) # point-to-point cost
    with torch.no_grad(): # the calculation involves momentum encoder, so with no grad here.
        # calculate the conditional transport map: M x K
        weights_for_pos = torch.softmax(cost_for_pos.mul(t_pos), dim=1) # calculate the positive transport map
    # calculate the positive transport with the empirical mean
    CCT_loss_pos += (cost_for_pos*weights_for_pos).sum(1).mean()

    ##### compute the loss of negative samples #####
    # calculate the cost and weights of negative samples from the queue: M x K
    sq_dists_for_cost = (2 - 2 * mm(q, queue))
    sq_dists_for_weights = sq_dists_for_cost

    if with_intra_batch: # compute the distance of negative samples in the mini-batch: Mx(M-1)
        intra_batch_sq_dists = torch.norm(q[:,None] - q, dim=-1).pow(2).masked_select(~torch.eye(q.shape[0], dtype=
            bool).cuda()).view(q.shape[0], q.shape[0] - 1)
        # combine the distance of negative samples from the queue and intra-batch: Mx(K+M-1)
        sq_dists_for_cost = torch.cat([sq_dists_for_cost, intra_batch_sq_dists], dim=1)
        sq_dists_for_weights = torch.cat([sq_dists_for_weights, intra_batch_sq_dists], dim=1)

    # calculate the negative transport map: if with_intra_batch==True Mx(K+M-1), else MxK
    weights_for_neg = torch.softmax(sq_dists_for_weights.mul(-t_neg), dim=1)
    # calculate the negative transport with the empirical mean
    CCT_loss_neg += (sq_dists_for_cost.mul(-1.0)*weights_for_neg).sum(1).mean()

    # combine the loss of positive transport and negative transport and update main encoder
    CCT_loss = CCT_loss_pos/len(im_list)+CCT_loss_neg/len(im_list)
    CCT_loss.backward()
    update(encoder_q.params) # SGD update: main encoder
    encoder_k.params = m*encoder_k.params+(1-m)*encoder_q.params #momentum update: key encoder

    # update the dictionary, dequeue and enqueue
    enqueue(queue, k_list[-1]) # enqueue the current minibatch
    dequeue(queue) # dequeue the earliest minibatch

```

pow: power function; mm: matrix multiplication; cat: concatenation.

Table 6: The top-1 classification accuracy (%) of different contrastive objectives with SimCLR framework on small-scale datasets. All methods follow SimCLR setting and apply a ResNet50 encoder and trained with 400 epochs.

Dataset	CL	AU-CL	HN-CL	CCT(K=1)	CMC(K=4)	CCT(K=4)
CIFAR-10	88.70	88.63	89.02	90.97	90.05	92.89
CIFAR-100	62.00	62.57	62.96	62.98	65.19	66.52
STL-10	84.60	83.81	84.29	88.42	91.40	93.04

C Additional Experiment Results

In this section, we provide additional results in our experiments, including ablation studies, and corresponding qualitative results.

C.1 Results with ResNet50 on small-scale datasets

As an additional results on small-scale datasets, we test the performance of CCT with ResNet50 as a different encoder backbone. Here we strictly follow the same setting of [Robinson et al. \(2021\)](#), and the results are shown in Table 6. We can observe with ResNet50 encoder backbone, CCT with single positive or multiple positive pairs consistently outperform the baselines.

C.2 On the Effects of Conditional Transport Map

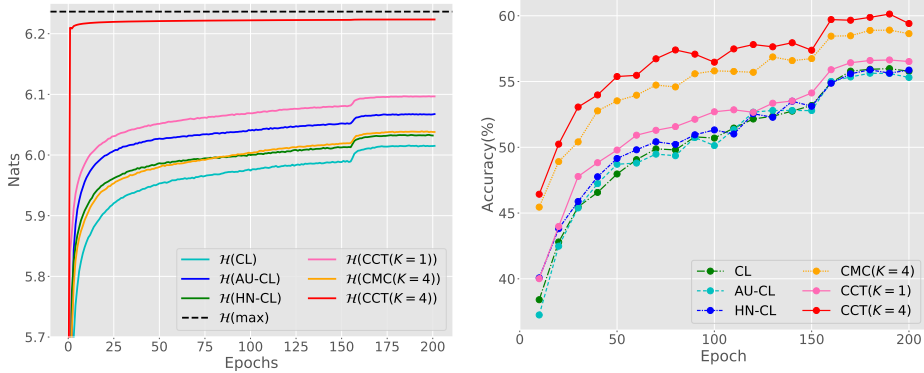
In order to further explore the effects of the conditional transport map, we conduct an ablation study to compare the performance of different variants of CCT with/without conditional transport maps. Here, we compare 4 configurations of CCT ($K = 4$): (i) CCT with both positive and negative transport maps; (ii) CCT without the positive transport map; (iii) CCT without the negative transport map; (iv) CCT without both positive and negative transport, which refers to conditional uniform transport model (CUT, see Equation 2). As shown in Table 7, when discarding the positive transport map, the linear classification accuracy slightly drops. As the negative transport map is discarded, there is a large performance drop compared to the full CCT objective. With the modeling of neither positive nor negative transport map, the CUT shows a continuous performance drop, suggesting that the success of representation learning is not guaranteed by uniformly pulling positive samples closer and pushing negative samples away. The comparison between these CCT variants shows the necessity of modeling the transport map.

Table 7: Linear classification performance (%) of different variants of our method. ‘‘CCT’’ represents the normal CCT configuration, ‘‘w/o π_{θ}^+ ’’ means without the positive transport map, ‘‘w/o π_{θ}^- ’’ means without the negative transport map. ‘‘CUT’’ indicates the conditional uniform transport (see the model we discussed in Equation 2), *i.e.* without both positive and negative transport map. This experiment is done on all small-scale datasets, with $K = 4$ and mini-batch size $M = 128$.

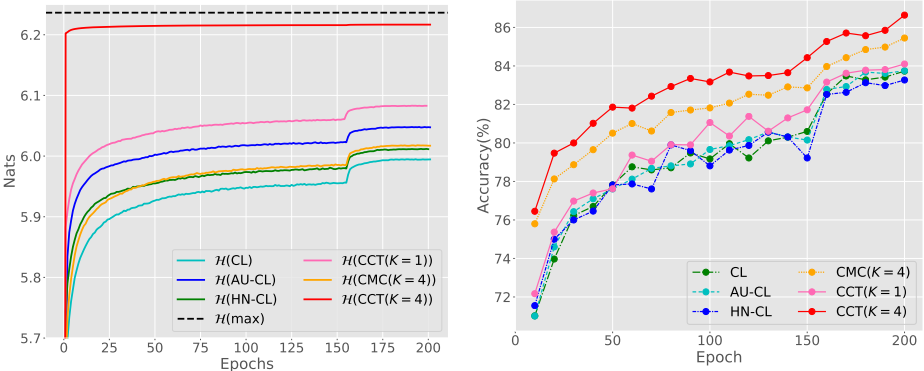
Methods	CIFAR-10	CIFAR-100	STL-10
CCT	85.94	59.51	85.59
w/o π_{θ}^+	85.22	58.74	85.06
w/o π_{θ}^-	78.49	47.88	72.94
CUT	77.17	44.24	71.88

As a continuous ablation study shown in Figure 3, we also conduct similar experiments on CIFAR-100 and STL-10, where we study the evolution of conditional entropy $\mathcal{H}(X^-|X)$ and classification accuracy *w.r.t.* the training epoch. Remind in each epoch, we calculate the conditional entropy with (11) on every mini-batch of size $M = 512$ (the last mini-batch will be ignored if the size is not 512) and take the average across the mini-batches. The results are shown in Figure 5. Similar to the observation on CIFAR-10, shown in Figure 3, we can observe $\mathcal{H}(X^-|X)$ is getting maximized as the encoder is getting optimized with these methods, which confirms Lemma 1. On the right panels, the linear classification results with learned representations is plotted every 10 epochs. We can observe CCT consistently provides better performance than the other methods at the same epoch, indicating the efficiency of CCT.

As qualitative illustrations, we randomly fix one mini-batch, and randomly select one sample as the query. Then we extract the features with the encoder trained with CL loss and CCT ($K = 1$) loss at epochs 1, 20, and 200, and visualize the (four) positives and negatives in the embedding space



(a) Entropy and classification accuracy *w.r.t.* epoch (CIFAR-100)



(b) Entropy and classification accuracy *w.r.t.* epoch (STL-10)

Figure 5: (*Supplementary to Figure 3*) Training evolution on CIFAR-100 and STL-10, with mini-batch size 512. **Left:** Conditional entropy $H(X^-|X)$ *w.r.t.* training epoch. The maximal possible conditional entropy is indicated by a dotted line. **Right:** Linear classification with learned representations *w.r.t.* training epoch.

Table 8: The top-1 classification accuracy (%) of different contrastive objectives with SimCLR framework on small-scale datasets. All methods follow SimCLR setting and apply a ResNet50 encoder and trained with 400 epochs.

Dataset	Trained with 400 epochs				Trained with 200 epochs	
	CL	AU-CL	HN-CL	CCT(K=1)	CMC(K=4)	CCT(K=4)
CIFAR-10	83.61	83.57	83.72	83.86	85.54	86.54
CIFAR-100	55.41	56.07	55.80	56.41	58.64	59.41
STL-10	83.49	83.43	82.41	83.56	84.50	85.59

with *t*-SNE (van der Maaten & Hinton, 2008). For more clear illustration, we center the query in the middle of the plot and only show samples appearing in the range of $[-10, 10]$ on both x and y axis. The results are shown in Figure 6(c), from which we can find that as the encoder is getting trained, the positive samples are aligned closer and the negative samples are pushed away for both methods. Compared to the encoder trained with CL, we can observe CCT shows better performance in achieving this goal. Moreover, we can observe the distance between any two data points in the plot is more uniform, which confirms that CCT shows better results in the maximization of the conditional entropy $H(X^-|X)$.

C.3 Ablation Study

Does CCT($K \geq 2$) outperform by seeing more samples? To address this concern, in our main paper, we intentionally decrease the mini-batch size as $M = 128$. Thus the total number of samples used per iteration is not greater than those used when $K = 1$. To further justify if the performance boost comes from seeing more samples when using multiple positive pairs, we also let the methods allowing single positive pair train with double epochs. As shown in Table 8, we can observe even trained with 400 epochs, the performance of methods using single positive pair still have a gap from those using multiple positive pairs.

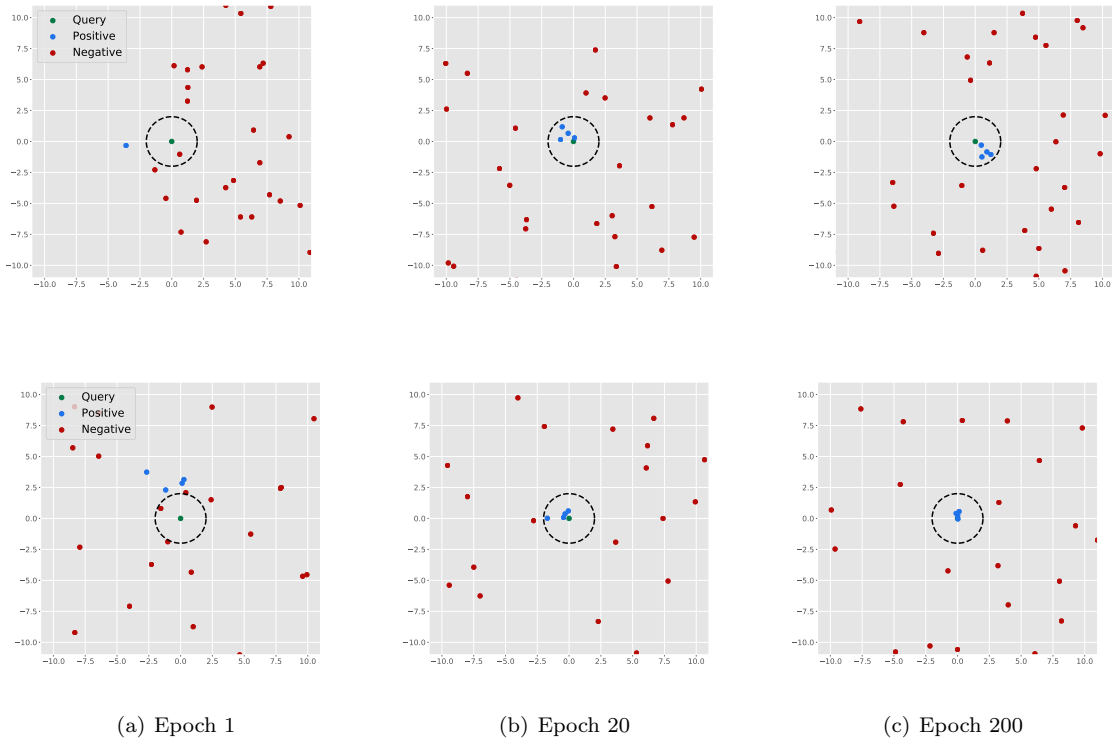


Figure 6: The t -SNE visualization of the latent space at different training epochs, learned by CL loss (top) and CCT loss (bottom). The picked query is marked in green, with its positive samples marked in blue and its negative samples marked in red. The circle with radius t^- is shown as the black dashed line. As the encoder gets trained, we can observe the positive samples are aligned closer to the query (Property 1), and the conditional differential entropy $\mathcal{H}(X^-|X)$ is progressively maximized, driving the distances $d(f_{\theta}(\mathbf{x}), f_{\theta}(\mathbf{x}^-))$ towards uniform (Lemma 1).

On the Effects of Sampling Size: We investigate the model performance and robustness with different sampling size by varying the mini-batch size used in the training. On all the small-scale datasets, the mini-batches are applied with size 64, 128, 256, 512, 768 and the corresponding linear classification results are shown in Figure 7. From this figure, we can see that CCT ($K = 4$) consistently achieves better performance than other objectives. For example, when mini-batch size is 256, CCT ($K = 4$) outperforms CMC by about 0.4%-1.2%. CCT ($K = 1$) shows better performance in most of the cases, while slightly underperforms than the baselines with mini-batch size 64. A possible explanation could be the estimation of the transport maps needs more samples to provide good guidance for the encoder.

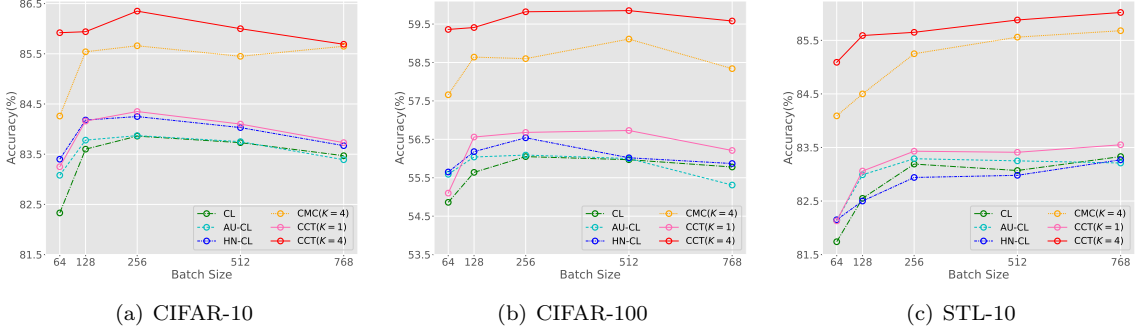


Figure 7: The linear classification results of training with different sampling size on small-scale datasets. The training batch size is proportional to the negative sampling size.

On the Effects of Hyper-parameter t^+ , t^- : Remind in the definition of positive and negative transport map, two hyper-parameters t^+ and t^- are involved as following:

$$\pi_{\theta}^+(\mathbf{x}^+ | \mathbf{x}, \mathbf{x}_0) := \frac{e^{t^+ \|\mathbf{f}_{\theta}(\mathbf{x}), \mathbf{f}_{\theta}(\mathbf{x}^+)\|^2} p(\mathbf{x}^+ | \mathbf{x}_0)}{\int e^{t^+ \|\mathbf{f}_{\theta}(\mathbf{x}), \mathbf{f}_{\theta}(\mathbf{x}^+)\|^2} p(\mathbf{x}^+ | \mathbf{x}_0) d\mathbf{x}^+}; \quad \pi_{\theta}^-(\mathbf{x}^- | \mathbf{x}) := \frac{e^{-t^- \|\mathbf{f}_{\theta}(\mathbf{x}), \mathbf{f}_{\theta}(\mathbf{x}^-)\|^2} p(\mathbf{x}^-)}{\int e^{-t^- \|\mathbf{f}_{\theta}(\mathbf{x}), \mathbf{f}_{\theta}(\mathbf{x}^-)\|^2} p(\mathbf{x}^-) d\mathbf{x}^-}.$$

In this part, we investigate the effects of t^+ and t^- on representation learning performance on small-scale datasets, with mini-batch size 768 ($K = 1$) and 128 ($K = 4$) as an ablation study. We search in a range $\{0.5, 0.7, 0.9, 1.0, 2.0, 3.0\}$. The results are shown in Table 9 and Table 10.

Table 9: The classification accuracy(%) of CCT ($K = 4$, $M = 128$) with different hyper-parameters t^+ on small-scale datasets.

Method	Dataset	0.5	0.7	0.9	1.0	2.0	3.0
CCT ($K = 4$)	CIFAR-10	86.07	85.78	85.90	86.54	84.85	84.76
	CIFAR-100	59.47	59.61	59.41	59.41	57.82	57.55
	STL-10	85.90	85.91	85.81	85.59	85.65	85.14

Table 10: The classification accuracy(%) of CCT ($K = 1$, $M = 768$) and CCT ($K = 4$, $M = 128$) with different hyper-parameters t^- on small-scale datasets.

Methods	Dataset	0.5	0.7	0.9	1.0	2.0	3.0
CCT ($K = 1$)	CIFAR-10	81.66	82.40	83.07	82.74	83.73	83.11
	CIFAR-100	51.42	52.81	53.36	54.20	56.21	56.52
	STL-10	80.37	81.47	81.89	82.16	83.55	83.90
CCT ($K = 4$)	CIFAR-10	85.67	86.19	86.54	86.41	85.94	85.69
	CIFAR-100	58.17	58.63	59.37	59.35	59.41	59.31
	STL-10	83.81	84.42	84.71	85.25	85.59	85.41

As shown in these two tables, from Table 9, we observe the CCT shows better performance with smaller values for t^+ . Especially when t^+ increases to 3.0, the performance drops up to about 1.9% on CIFAR-100. For analysis, since we have $K = 4$ positive samples for the computation of positive transport map, using a large value for t^+ could result in an over-sparse transport map, where

the transport probability is dominant by one or two positive samples. This also explains why the performance when $t^+ = 3.0$ is close to the classification accuracy of CCT ($K = 1$).

Similarly, from Table 10, we can see that a small value for t^- will lead to the degenerated performance. Here, since we are using mini-batches of size 768 ($K = 1$) and 128 ($K = 4$), a small value for t^- will flatten the weights of the negative pairs and make the transport map closer to a uniform distribution, which explains why the performance when $t^- = 0.5$ is close to those without modeling π_{θ}^- . Based on these results, the values of $t^+ \in [0.5, 1.0]$ and $t^- \in [0.9, 2.0]$ could be good empirical choices according to our experiment settings on these datasets.

C.4 Results of Different Cost Metrics

Recall that the definition of the point-to-point cost metric is usually set as the quadratic Euclidean distance:

$$c(f_{\theta}(\mathbf{x}), f_{\theta}(\mathbf{y})) = \|f_{\theta}(\mathbf{x}) - f_{\theta}(\mathbf{y})\|_2^2. \quad (15)$$

In practice, the cost metric defined in our method is flexible to be any valid metrics. Here, we also investigate the performance when using the Radial Basis Function (RBF) cost metrics:

$$c_{\text{RBF}}(f_{\theta}(\mathbf{x}), f_{\theta}(\mathbf{y})) = -e^{-t\|f_{\theta}(\mathbf{x}) - f_{\theta}(\mathbf{y})\|_2^2}, \quad (16)$$

where $t \in \mathbb{R}^+$ is the precision of the Gaussian kernel. With this definition of the cost metric, our method is closely related to the baseline method AU-CL (Wang & Isola, 2020), where the authors calculate pair-wise RBF cost for the loss *w.r.t.* negative samples. Following Wang & Isola (2020), we replace the cost metric when calculate the negative transport with the RBF cost and modify $\hat{\mathcal{C}}^-$ as:

$$\begin{aligned} \hat{\mathcal{C}}_{\text{RBF}}^- &:= \ln \left[\frac{1}{M} \sum_{i=1}^M \sum_{j \neq i} \frac{e^{-d_{t^-}(f_{\theta}(\mathbf{x}_i), f_{\theta}(\mathbf{x}_j))}}{\sum_{j' \neq i} e^{-d_{t^-}(f_{\theta}(\mathbf{x}_i), f_{\theta}(\mathbf{x}_{j'}))}} \times c_{\text{RBF}}(f_{\theta}(\mathbf{x}_i), f_{\theta}(\mathbf{x}_j)) \right] \\ &= \ln \left[\frac{1}{M} \sum_{i=1}^M \sum_{j \neq i} \frac{e^{-d_{t^-}(f_{\theta}(\mathbf{x}_i), f_{\theta}(\mathbf{x}_j))}}{\sum_{j' \neq i} e^{-d_{t^-}(f_{\theta}(\mathbf{x}_i), f_{\theta}(\mathbf{x}_{j'}))}} \times e^{-t\|f_{\theta}(\mathbf{x}_i) - f_{\theta}(\mathbf{x}_j)\|_2^2} \right]. \end{aligned} \quad (17)$$

Here the negative transport is in log scale for numerical stability. When using the RBF cost metric, we use the same setting in the previous experiments and evaluate the linear classification on all small-scale datasets. The results of using Euclidean and RBF cost metrics are shown in Table 11. From this table, we see that both metrics achieve comparable performance, suggesting the RBF cost is also valid in our framework. In CCT, the cost metric measures the transport cost of different sample pairs and is not limited on specific formulations. More favorable cost metrics can be explored in the future.

Table 11: The classification accuracy (%) of CCT ($K = 1$) and CCT ($K = 4$) with different cost metrics on CIFAR-10, CIFAR-100 and STL-10. Euclidean indicates the cost defined in Equation 15, and RBF indicates the cost metrics defined in Equation 16.

Methods	Cost Metric	CIFAR-10	CIFAR-100	STL-10
CCT($K = 1$)	Euclidean	83.73	56.21	83.55
	RBF	83.08	55.90	84.20
CCT($K = 4$)	Euclidean	85.94	59.41	85.59
	RBF	86.20	58.81	85.80